

Multiresolution Mapping of Land Cover From Remote Sensing Images by Geometric Generalization

Yilang Shen^{ID}, Jingzhong Li, Rong Zhao, and Fengfeng Han

Abstract—Land cover multiresolution mapping of remote sensing images contributes greatly to land-use management, environmental protection, and city planning. In traditional mapping of this type, the representation of different land-use types depends on the image resolution, and the geometric, topologic, and semantic characteristics are not considered. This approach can cause a loss of useful information and the redundancy of useless information. In this study, we propose a superpixel-based land cover (multiresolution representation SULR) method for remote sensing images that employs multifeature fusion. In this process, we first define three basic superpixel operations, collapse, connection, and cutting, as the basic operators of multiresolution land cover mapping. Then, the topological adjacent land parcels are combined through the amalgamation of polygons with heterogeneous properties and aggregation of polygons with homogeneous properties based on the three proposed superpixel operators. Finally, the geometric boundaries of parcels are simplified by combining the superpixel collapse operator and image thinning technologies. Compared with traditional image scale transformation methods, the proposed method can more effectively achieve multiresolution mapping of land cover from remote sensing images by considering the geometric, topologic, and semantic characteristics of land parcels.

Index Terms—Land cover, multiresolution mapping, remote sensing images, superpixel segmentation.

I. INTRODUCTION

LAND cover mapping from remote sensing images is very important in many fields, including urban construction and planning, land resource administration, agricultural production, and environmental conservation [1]–[6]. Multiresolution representation of land-use maps is necessary because

Manuscript received November 26, 2020; revised March 26, 2021; accepted April 26, 2021. Date of publication May 14, 2021; date of current version December 29, 2021. This work was supported in part by the National Key Research and Development Program of China under Grant 2017YFB0503601 and Grant 2017YFB0503502; in part by the National Natural Science Foundation of China under Grant 42001402; in part by the National Natural Science Foundation of China under Grant 41671448; in part by the Key Research and Development Program of Sichuan Province under Grant 19ZDYZF0839; in part by the Natural Science Foundation of Hubei Province under Grant 2018CFB162; and in part by the National Key Research and Development Program of China under Grant 2017YFB0503500. (Corresponding author: Jingzhong Li.)

Yilang Shen and Jingzhong Li are with the School of Resource and Environmental Sciences, Wuhan University, Wuhan 430072, China (e-mail: 00009232@whu.edu.cn).

Rong Zhao is with the Institute of Cartography and Geographic Information System, Chinese Academy of Surveying and Mapping, Beijing 100830, China.

Fengfeng Han is with Wuda Geo Information Technology Controls Ltd., Wuhan 430223, China.

Digital Object Identifier 10.1109/TGRS.2021.3076798

geographic scale provides a constraint definition for our Earth observations [7] and affects many processes, such as land data transfer, aggregation, and analysis [8]. As different cartographers using the same basic data can generate land cover maps with differences, automatic techniques for generating multiresolution land cover data are always applied to avoid inconsistency problems [9].

In the multiresolution mapping of land cover, several important issues should be resolved [10]–[13].

- 1) **Aggregation of Polygons With Homogeneous Semantics:** In this process, multiple polygons that are short distances apart should be merged into one larger polygon.
- 2) **Amalgamation of Polygons With Heterogeneous Semantics:** In this process, a small polygon can be merged into multiple adjacent polygons with heterogeneous semantics via division into several different patches. In this process, the topologic relationships should be maintained.
- 3) **Geometric Simplification of Polygon Boundaries:** This step is applied to remove the details of the boundaries of polygons when the map scale decreases. The original topological relationships of polygons should be maintained during this process.

Although traditional raster-based scale mapping of land cover from remote sensing images can be realized using sampling and filtering methods, such as nearest-neighbor interpolation (NNI), bilinear interpolation, and median filtering (MF) methods [14], [15], they process map elements only at the pixel level, and geometric, topologic, and semantic characteristics cannot be considered in this process. As an example, Fig. 1(a)–(c) shows a multiresolution representation of land cover using NNI, in which the noise in the original classification map is reduced using filtering operations. Although transformation can be realized at different levels of detail [Fig. 1(a)–(c)], the details of boundaries that are difficult to distinguish visually cannot be removed, which may lead to poor visual effects compared with the rightmost result of boundary simplification [Fig. 1(d)]. The MF method can simplify the details of boundaries; however, as shown in Fig. 1(e)–(g), this method can also generate new regions with different colors (marked with red circles), fractures (marked with red arrows), and long narrow regions (marked with red ellipses). In this process, the original topological relationships cannot be well maintained since they can generate redundant

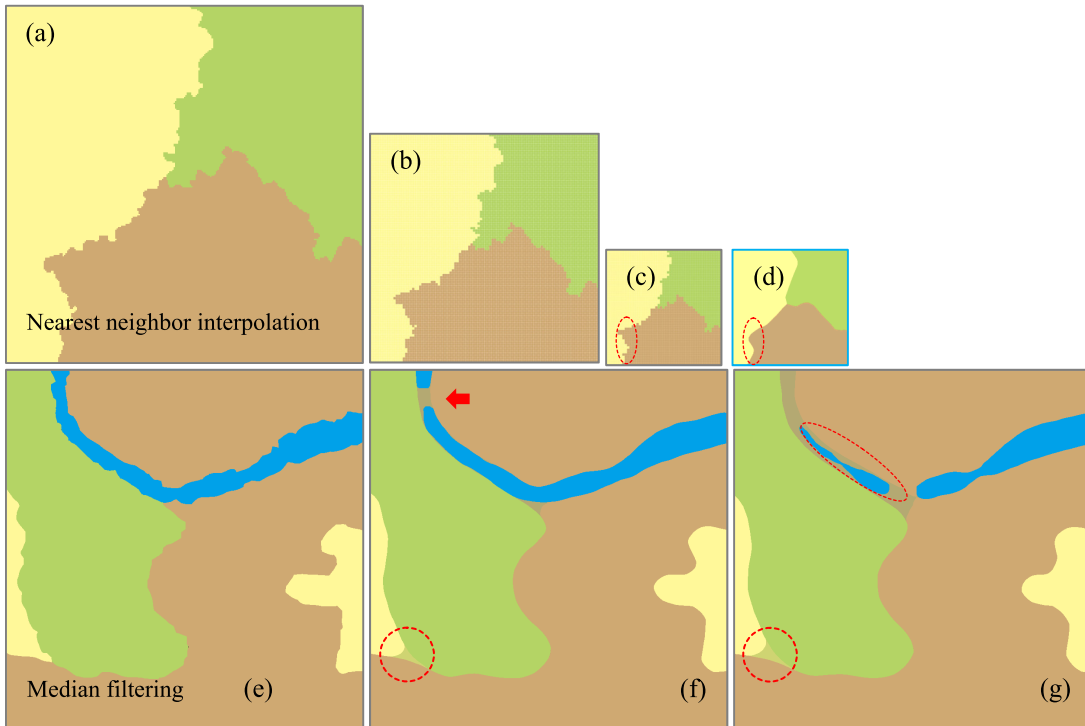


Fig. 1. Multiresolution mapping of land cover using traditional image processing methods. (a)–(c) Nearest-neighbor interpolation. (d) Boundary simplification. (e)–(g) Median filtering.

regions at the intersection of multiple patches, and the long narrow regions cannot be well merged into adjacent patches.

Some scholars have proposed vector-based methods as an alternative to traditional methods for land cover multiscale mapping [6], [10], [16], [17]. For example, Haunert and Wolff [9] proposed an approach for the automatic generalization of vector land cover maps based on a mixed integer program, which can maintain the original topologic relationships and minimal changes in land cover classes. However, these vector-based methods cannot be directly applied to remote sensing images since the data structures of raster and vector data are very different. To realize the scale transformation of land cover from remote sensing images using vector-based methods, we have to perform multiple steps, including multiresolution image processing, vectorization of raster images, and land cover generalization. This division of tasks can result in a relatively long production period, complex operational processes, and large errors in accuracy. There is an urgent need to simplify these separate mapping processes to promote their integration and streamline the task of multiresolution land cover mapping from remote sensing images.

Therefore, in this study, by combining modern computer vision technologies, we attempt to directly generate multiresolution land cover maps from remote sensing images via the fusion of geometric, topologic, and semantic characteristics. In the meantime, solving the above three key problems, namely aggregation, amalgamation, and simplification of land patches, based on raster data are also the main targets of this study.

This article is organized as follows. Section II describes the related work regarding the scale transformation of land cover, including raster-based and vector-based methods. Section III

describes the methods for multiresolution mapping of land cover from remote sensing images. A technical framework for multiresolution mapping of land cover is proposed, and a multiresolution cartographic representation of land cover in remote sensing images is realized based on the proposed framework, which mainly includes land cover classification, aggregation, amalgamation, and simplification of raster land cover polygons. In Section IV, high-resolution submeter remote sensing images are used to assess the proposed methods, and the original experimental data, processing procedure, experimental results, and discussion are described. Section V describes the conclusions and future work.

II. RELATED WORKS

A. Raster-Based Methods

In the field of image processing, the typical scale transformation of images includes image interpolation methods, such as nearest neighbor, bilinear, bicubic, and Lanczos interpolation [14], [15], and image pyramid methods, such as Gaussian pyramid and Laplacian pyramid [18], [19]. Image interpolation aims to achieve the best pixel intensity estimation by calculating the proximity pixel analysis. To satisfy the specifications of image mapping or visual readability of image representation, image interpolation during the image resizing process is necessary. The basic interpolation approach is the NNI, in which the generated pixel values are calculated from the values of the nearest pixels. This method is easy and simple to perform, and the final results contain no artificial data. However, the results from NNI can generate blocking artifacts, which may lead to large errors in performance evaluation. The bicubic interpolation method can generate smoother

representations from the original image, but the efficiency is relatively low.

Another important image scale transformation technique is the image pyramid, which usually contains a Gaussian pyramid and Laplacian pyramid. An image pyramid is composed of a series of successively sampled images with different resolutions generated from an original image [18], [19]. The Gaussian pyramid and Laplacian pyramid are usually applied to downsampled (zoomed-out view) and upsampled (zoomed-in view) images. For example, the Gaussian pyramid can perform low pass filtering operation for the original image to generate a reduced image with both lower spatial resolution and density. The low pass filtering operation is realized using a convolution by a Gaussian distribution weighting function. In addition, many scholars have proposed methods for simplified representation of linear features [20]–[26] and areal features [27]–[29] based on image processing technology. For example, Bhowmick and Bhattacharya [22] developed a method to extract digital straight line segments based on the definition of approximate straightness. This method can effectively realize polygonal approximation with a high speed. Shen *et al.* [24] proposed a line simplification method based on corner detection and minimum-perimeter polygon technologies. They applied this method for the simplification of water area boundaries, and the results indicated that the positional accuracy of local features of the water area boundaries can be maintained.

Although scale transformation methods exist for images, they are not appropriate for multiresolution mapping of land cover because the geometric, topologic, and semantic characteristics cannot be properly considered when using these methods.

B. Vector-Based Methods

In the field of vector map multiresolution representation, some scholars have proposed methods for the generalization of land cover [9], [16], [17]. For example, Ai and Liu [16] proposed a method for solving aggregation and amalgamation problems in land cover data generalization based on the Voronoi diagram model. This method considers both semantic and spatial issues during land cover generalization. Guo *et al.* [17] developed a method for land cover data generalization by introducing thematic knowledge, such as application-specific, culture-, and nature-based knowledge. In this study, they analyzed and collected thematic knowledge of land cover generalization as much as possible and controlled the generalization process by formalizing knowledge to rules. The results indicated that the knowledge-based method is efficient for land cover data generalization and is easy to implement.

In addition, some separated algorithms, including aggregation [11]–[13], [30], [31], amalgamation [32], general boundary simplification [33]–[43], and building simplification algorithms [44]–[46], which can be used for vector generalization land cover boundaries, are proposed.

Based on the above analysis, the following three gaps in traditional multiresolution mapping of land cover from remote sensing images are observed.

- 1) As multiresolution mapping of land cover is a complicated process that contains multiple operations, such as aggregation, amalgamation, and simplification, there is no complete technical framework for multiresolution mapping of land cover from remote sensing images.
- 2) Although there are multiple multiresolution mapping methods based on vector data, only a limited number of methods based on raster data are available. Vector-based methods cannot be applied to remote sensing images, and the existing raster-based methods have obvious drawbacks. For example, interpolation methods can be used to shrink images, but these methods cannot simplify boundaries; MF methods can be used to simplify boundaries, but these methods cannot preserve the original topologic relationships. In other words, these methods only process map elements at the pixel level and the geometric, topologic, and semantic characteristics cannot be considered in this process.
- 3) There is a lack of raster-based land cover multiresolution mapping methods, and there is an urgent need to develop them. For example, the raster-based amalgamation method is lacking.

As the land cover classification technologies from images are already very mature, in this study, we focus mainly on filling the above three gaps for multiresolution land cover mapping from remote sensing images.

III. METHODS FOR MULTIRESOLUTION LAND COVER MAPPING FROM REMOTE SENSING IMAGES

The overall framework for multiresolution mapping of land cover from remote sensing images based on the proposed superpixel-based land cover multiresolution representation (SULR) method is shown as a detailed flowchart in Fig. 2. First, using the input remote sensing images, land cover classification preprocessing is performed. Then, a multilevel transformation is realized based on the proposed SULR method, which mainly involves aggregation, amalgamation, and simplification of land cover. In this process, we define three basic superpixel operations, collapse, connection, and cutting, according to the differences in the semantic types of land cover; this procedure is the theoretical basis for multilevel transformation and is described in detail in Section III-B. For land parcels with heterogeneous semantics, the amalgamation described in detail in Section III-C should be performed, which mainly involves linear spectral clustering (LSC) segmentation, corner detection, superpixel collapse, and cutting operations. For the land parcels with homogeneous semantics, the aggregation described in detail in Section III-D should be performed, which mainly involves LSC segmentation, corner detection, superpixel connection, and cutting operations. For the land parcel boundaries, the simplification described in detail in Section III-E should be performed, which mainly entails global and local simplification realized by LSC segmentation, superpixel collapse, MF, and image thinning. During this process of multilevel transformation, we consider various constraint criteria, including topological, geometrical,

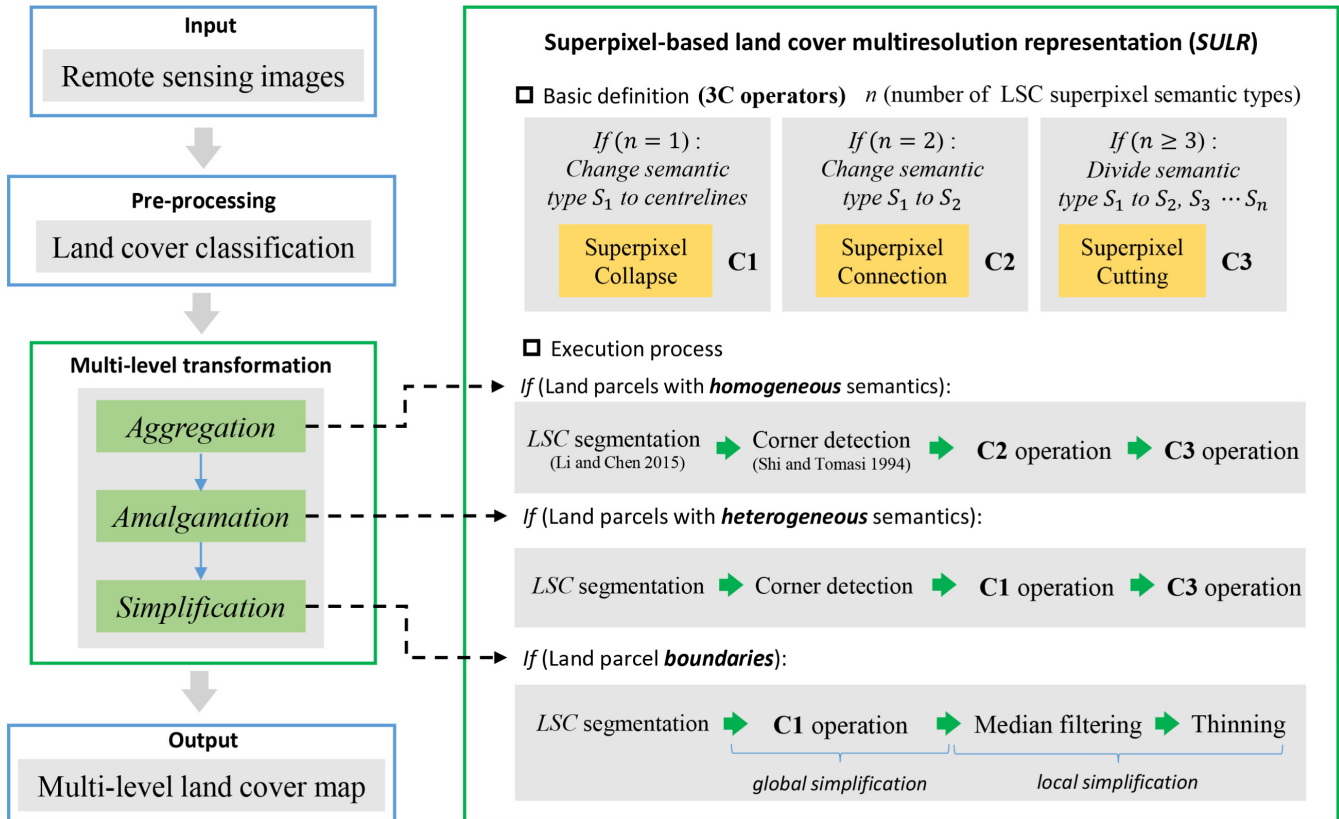


Fig. 2. Overall framework presented as a detailed flowchart for the multiresolution mapping of land cover from remote sensing images using the proposed SULR method.

and semantic characteristics of land cover. Finally, a land cover map is generated at different levels of detail.

A. Classification of Land Cover

As land cover classification from remote sensing images is a popular research topic, many scholars have proposed various methods for achieving it [6], [47]–[49]. In recent years, deep learning technologies have made it possible to realize high-accuracy classification of land cover from high-resolution remote sensing images. For example, Tong *et al.* [6] applied transferable deep models for land cover classification, which achieved an overall classification accuracy and Kappa coefficient of the experimental areas of 94.56% and 0.924, respectively. Thus, in this article, we do not provide further analysis on land cover classification but rather focus on the multiresolution transformation of land cover after classification from remote sensing images.

B. Definition of Basic Superpixel Operations

To realize the multiresolution representation of land cover data generated from remote sensing images, we first introduced the superpixel as the basic transformation operation unit. Ren and Malik [50] first proposed the superpixel definition in 2003. Superpixels are adjacent pixel sets with similar properties, including textures, colors, intensities, or other characteristics. In this study, we applied the LSC method [51] to generate

basic superpixels. As shown in Fig. 3, based on the superpixel structure, we defined three basic superpixel operations: collapse, connection, and cutting (3C operators) as follows.

Collapse is a dimension reduction operation of superpixels. The lines generated from the center points of adjacent superpixels with the same semantic type S_a according to certain rules will replace the original areal regions composed of these superpixels. For example, in Fig. 3(a), using the collapse operator, a new line that is connected by the center points of the superpixels with the water (blue) property is generated.

Connection is a combination operation of superpixels. Assuming that superpixel A is generated from the object with semantical type S_a , when superpixel A connects two (or more) other superpixels with the same semantics type S_b , the semantic type of superpixel A will be changed to S_b . For example, as shown in Fig. 3(b), as superpixel A with a shrub (orange) property connects two superpixels B and C with a forest (green) property, by using the connection operator, the property of superpixel A will be changed to the forest (green) property.

Cutting is a division operation of superpixels. Assuming that superpixel A is generated from the object with semantic type S_a , when superpixel A connects two (or more) other superpixels with different semantic types S_b and S_c , the semantic type of superpixel A will be divided into two (or more) types of S_b and S_c according to certain division rules. For example, as shown in Fig. 3(c), using the cutting operator, the original

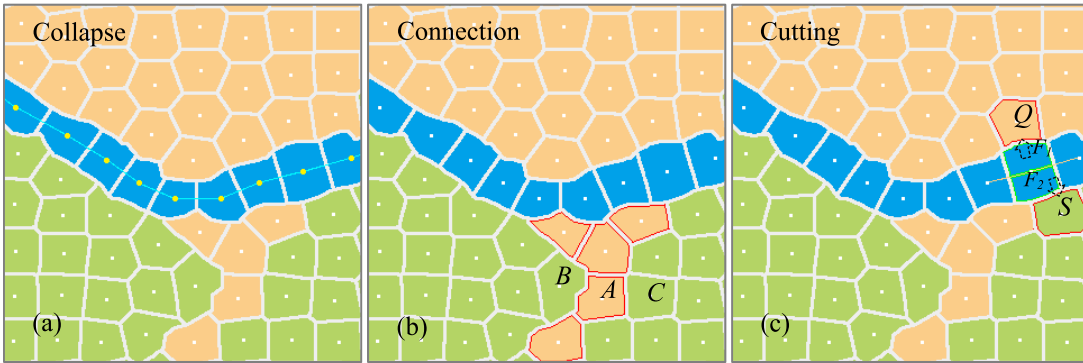


Fig. 3. Three types of superpixel operations: collapse, connection, and cutting. (a) Collapse. (b) Connection. (c) Cutting.

superpixel F with a water (blue) property is first divided into two parts F_1 and F_2 according to the lines generated from the center points of superpixels. Then, part F_1 will be merged into the adjacent superpixel Q with the shrub (orange) property, and part F_2 will be merged into the adjacent superpixel S with the forest (green) property.

The pseudocodes for the definition of basic superpixel operations are as follows.

Function Operations (Input superpixels S , semantic type number n)

Begin

#Collapse

if ($n = 1$) *then:*

perform connect the centrepoints of S
return centerlines of S

#Connection

if ($n = 2$) *then:*

perform change target semantic type T_1 to T_2
return S with semantic type T_2

#Cutting

if ($n \geq 3$) *then:*

perform divide target semantic type T_1 to T_2, T_3, \dots, T_n
return S with semantic type T_2, T_3, \dots, T_n

End

Using the above three basic superpixel operations, namely, collapse, connection, and cutting, the amalgamation, aggregation, and simplification of land cover data extracted from remote sensing images will be realized. In this process, some other assisted operations, such as corner detection, MF, and image thinning, are also integrated to generate the optimization results.

C. Amalgamation of Land Parcels With Heterogeneous Semantics

Amalgamation is a process of merging several adjacent polygons with various semantic types to a single polygon [10], [32]. Amalgamation can be applied to solve proximity conflicts that occur when gaps among polygon objects are too small to be visually identified. Usually, when a polygon x has n topological adjacent polygons y_1, y_2, \dots, y_n with different semantic information, it should be merged into the polygon y_n , which has the longest shared boundary [16], [31], [52]. To maintain uniformity during amalgamation, a better solution

is the method of the skeleton line division [16]. First, polygon x is split into n pieces using the skeleton lines generated from Delaunay triangulation. Then, each piece is merged into the corresponding adjacent polygon y_n . However, the amalgamation method based on Delaunay triangulation can only be applied to vector land cover data, and there is no available method for the image data. In this study, we developed an image-based amalgamation method of skeleton line division using the defined superpixel collapse and cutting operators. The main steps are described as follows.

First, corner detection is performed to determine the LSC superpixels that should be identified for the amalgamation operator. Usually, a character point possessing a local maximum intensity or maximal curvature can be defined as a corner. Over the past few years, many methods designed for corner detection have been developed [53]–[58]. In this study, the corner detection method proposed by Shi and Tomasi [59] is applied to detect the local characteristics of superpixels generated from land cover data. An example can be found in Fig. 4. Fig. 4(a) shows the LSC segmentation results of land cover data (image size: 825×825 pixels) with the superpixel size $S = 40$. The corresponding parameters used in corner detection are outlined as follows.

- 1) $ql = 0.1$: Parameter ql represents the quality level that characterizes the minimal accepted quality of detected corners.
- 2) $md = 20$: Parameter md represents the minimum Euclidean distance between the detected corners.
- 3) $bs = 8$: Parameter bs represents the block size used to compute a derivative covariation matrix in the neighborhood of each pixel.

As the corners extracted by the Shi and Tomasi method only reach the pixel level and the obtained corner coordinates are integers, to improve the accuracy of detected corners, an optimal computation at a subpixel accuracy level is applied [60]. After subpixel detection, the values at locations between integer pixels can be generated. For example, assuming that one corner coordinate generated from the Shi and Tomasi method is $(10, 20)$, the new coordinate at a subpixel accuracy level can be $(9.128, 20.252)$. Using subpixel optimization, the local redundant corners can be removed. Fig. 4(b) shows the results of superpixel corner detection. The red points represent the corners after subpixel detection.

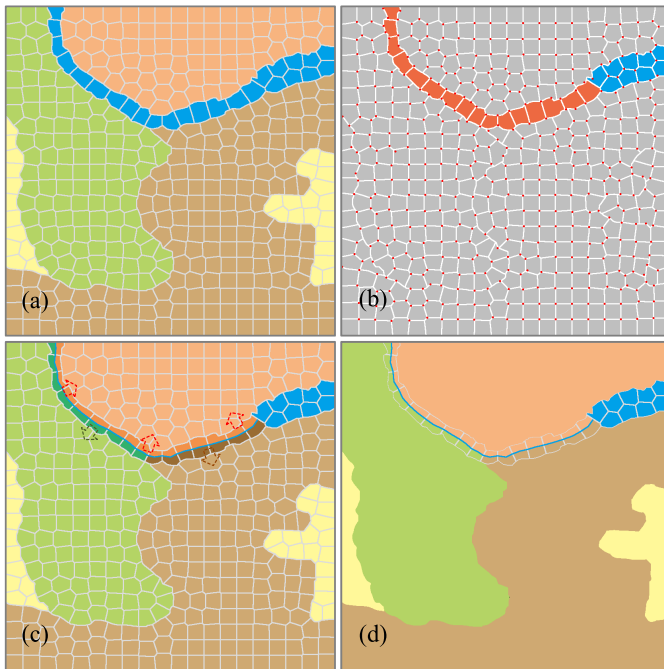


Fig. 4. Amalgamation of land parcels using superpixel collapse and cutting operators. (a) Superpixel segmentation. (b) Corner detection. (c) Cutting. (d) Collapse.

Then, a superpixel collapse operator is performed according to the following rules. When all the corners of one superpixel are located in the boundaries of the original polygons and this superpixel connects two (or more) other superpixels with different semantic types, this superpixel should be selected to perform the collapse operation. For example, the superpixels marked in orange in Fig. 4(b) are the selected superpixels. When some corners of one superpixel are located in the interior of the original polygons, this superpixel should not be selected. For example, the superpixels marked in blue in Fig. 4(b) are the superpixels that should not be selected. In Fig. 4(c), the blue line is the result of the superpixel collapse operation generated from the orange superpixels.

Finally, a superpixel cutting operator is performed according to the following rules. If a cutting superpixel piece generated from the centerlines connected by center points of superpixels has a common boundary with one adjacent superpixel, this superpixel piece should be merged to this adjacent superpixel. If a cutting superpixel piece has a common boundary with more than one adjacent superpixel, this superpixel piece should be merged to the adjacent superpixel with the longest common boundary. An example can be found in Fig. 4(c); the dark blue (brown and orange) superpixel pieces should be merged with the light blue (brown and orange) superpixels. Fig. 4(d) shows the final amalgamation result after a superpixel cutting operation.

The pseudocodes for the amalgamation of land parcels with heterogeneous semantics are as follows.

Function Amalgamation (*Input* land cover image I_0)

Begin

perform LSC superpixel segmentation of I_0 to generate superpixels S

perform corner detection for S

```

if (corners of  $S$  are located in the boundaries) and ( $S$ 
connects
superpixels with  $x$  semantic types) and ( $x \geq 2$ ) then:
  perform collapse operation for  $S$ 
  perform cutting operation for  $S$  to generate cutting
  superpixel piece  $P$ 
  if ( $P$  has a common boundary with  $y$  adjacent
  superpixels) and ( $y = 1$ ) then:
    perform merge  $P$  into this adjacent superpixel
  if ( $P$  has a common boundary with  $z$  adjacent
  superpixel) and ( $z \geq 1$ ) then:
    perform merge  $P$  into the adjacent superpixel with
    the longest common boundary
  return land cover image  $I_r$ 
End
```

Using the amalgamation method proposed in this study, land parcels with long and narrow shapes can be uniformly merged into adjacent parcels with heterogeneous semantics. In addition, during the amalgamation process, the original land parcels can be progressively recognized and collapsed according to width, the narrow parts can be replaced with linear features, and the wide parts can be preserved.

D. Aggregation of Land Parcels With Homogeneous Semantics

The aggregation operation is applied to merge polygons with homogeneous semantics that are not touching [10]. In this process, the gaps between polygons should be well connected. In traditional raster-based methods, mathematical morphology operators such as erosion and dilation can be used for polygon aggregation. However, the erosion and dilation operators can lead to a shape change in the original boundaries. In this study, a raster-based aggregation method using the defined superpixel connection and cutting operators is proposed as follows.

First, the corner detection described in Section III-C is performed to determine the LSC superpixels that should be identified for the superpixel aggregation operator. When all the corners of one superpixel are located along the boundaries of the original polygons and this superpixel connects only one type of superpixel with the same semantic types, this superpixel should be selected to perform the aggregation operation.

Then, a superpixel connection operator is performed. As shown in Fig. 5(a), as the orange superpixels with the original shrub property connect green superpixels with the forest property, the property of these orange superpixels, which can be called connected superpixels, will be changed to the same as the property of the green superpixels, which can be called target superpixels.

Finally, a superpixel cutting operator is performed according to the following rules. In this process, the cutting lines are not the centerlines connected by center points of superpixels but the lines located in the interior of the connected superpixels at two ends. If a connected superpixel has overlapping boundaries with adjacent superpixels that have two or more semantic types, this connected superpixel can be identified as an endpoint superpixel, such as superpixels m and n in

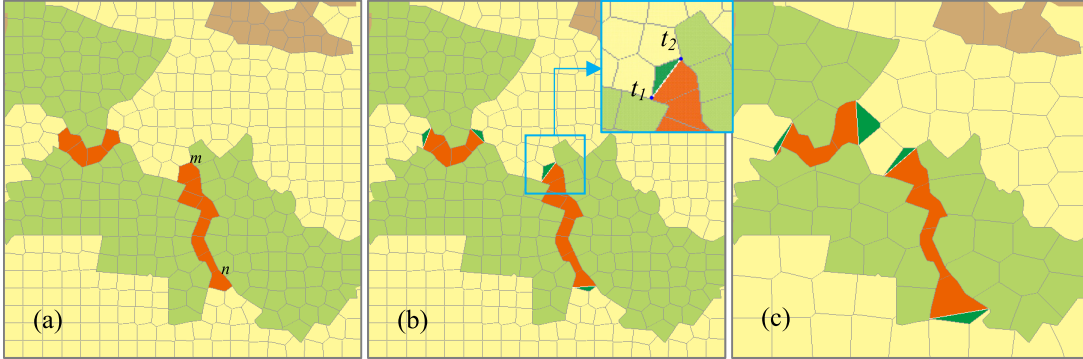


Fig. 5. Aggregation of land parcels using superpixel connection and cutting operators. (a) Connection. (b) Cutting. (c) Aggregation with increasing superpixel size.

Fig. 5(a). Assuming that superpixel T is an endpoint superpixel, the endpoints of the intersecting lines between endpoint superpixel T and the target superpixels should be connected as the cutting lines. For example, as shown in Fig. 5(b), the cutting line of an endpoint superpixel can be connected by the endpoints of t_1 and t_2 . According to the generated cutting lines, the endpoint superpixels can be divided into two parts: the part with overlapping boundaries with target superpixels should be merged, and the remaining part, such as the dark green parts in Fig. 5(b) and (c), should preserve the original property.

The pseudocodes for the aggregation of land parcels with homogeneous semantics are as follows.

```
Function Aggregation (Input land cover image  $I_0$ )
Begin
    perform LSC superpixel segmentation  $I_0$  to generate
    superpixels  $S$ 
    perform corner detection for  $S$ 
    if (corners of  $S$  are located along the boundaries) and ( $S$ 
    connects superpixels with the  $x$  semantic types) and ( $x =$ 
    1) then:
        perform connection operation for  $S$  to generate
        connected superpixel  $CS$ 
        perform cutting operation for  $S$  to generate endpoint
        superpixel  $ES$ 
        if (an  $CS$  is an  $ES$ ) then:
            perform property subdivision of  $ES$ 
    return land cover image  $I_r$ 
End
```

Using the aggregation method proposed in this study, the narrow gaps between land parcels with homogeneous semantics can be well connected, while the original boundary shape can also be well preserved. As shown in Fig. 5(c), with increasing superpixel size, gaps with wider distances are connected.

E. Simplification of Land Parcel Boundaries

Simplification operations can remove redundant details and preserve the main shape characteristics of polygon boundaries [22], [61]. For simplification of raster land parcel boundaries, it is difficult to preserve the original topological relationships using traditional image processing methods, such as MF or mathematical morphology technologies. In this study,

a raster-based simplification method of land parcel boundaries combining the defined superpixel collapse operator and MF is proposed as follows.

First, a global simplification using the superpixel collapse operator is performed to remove large curves. In this process, the outermost superpixels of each land parcel collapse to linear features by connecting the center points of superpixels, as shown by the green lines in Fig. 6(a) and (d).

Then, a local simplification using MF is performed to smooth small features. In this process, the areal regions generated from the collapsed linear features are smoothed by MF. For example, the gray area in Fig. 6(b) is the result of MF generated from the gray area in Fig. 6(a). After that, an image thinning operation [62] is performed to generate the final simplification results, such as the red lines in Fig. 6(c).

The pseudocodes for the simplification of land parcel boundaries are as follows.

```
Function Simplification (Input land cover image  $I_0$ )
Begin
    perform LSC superpixel segmentation  $I_0$  to generate super-
    pixels  $S$ 
    if (superpixel  $S$  is located outermost) then:
        perform collapse operator for  $S$ 
        perform median filtering
        perform thinning of outermost superpixels
    return land cover image  $I_r$ 
End
```

Using different superpixel sizes, simplification results with different granularities can be generated. For example, the superpixel sizes used in Fig. 6(a) and (d) are 30 and 60, respectively. The corresponding simplification results can be found in Fig. 6(d) and (f), from which we can see that with increasing superpixel size, larger curves are removed, such as the regions marked with circles. Compared with MF, such as the example in Fig. 1, the proposed method can remove larger curves and preserve the original topological relationships. In addition, it can avoid creating redundant areas because of fractures.

IV. EXPERIMENTS AND EVALUATIONS

A. Experimental Area

The experimental area used in this study comes from the DeepGlobe Land Cover Classification Challenge, which is

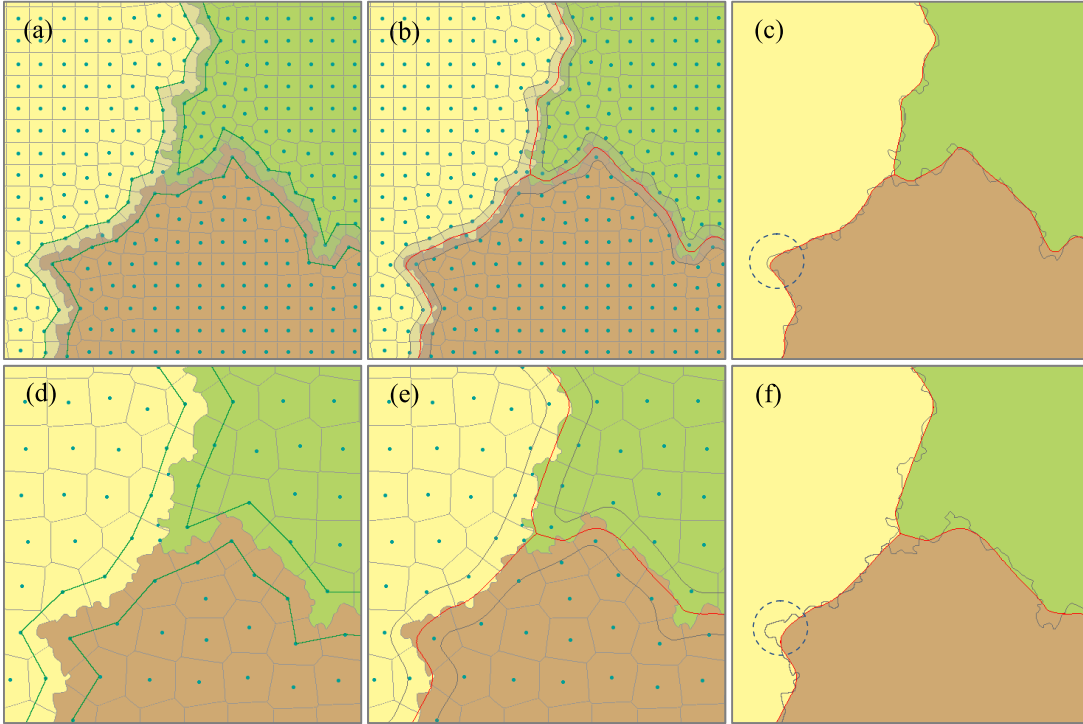


Fig. 6. Simplification of land parcel boundaries by combining the superpixel collapse operator and MF. Simplification with (a)–(c) smaller superpixels and (d)–(f) larger superpixels.

TABLE I
CLASSES OF THE DEEPGLOBE LAND COVER CLASSIFICATION DATASET

Class	Content	Relative percentage	Color
Agriculture land	Confined feeding operations, plantation, cropland, ornamental horticultural areas, orchards and farms	56.76%	Yellow
Forest land	Land possessing more than 20% density of tree crown	13.75%	Green
Rangeland	Non-farm, non-forest, grass and green land	10.21%	Red
Urban land	Artificial built up regions	9.35%	Cyan
Barren land	Land with no vegetation, rock, beach, mountain and dessert	6.14%	White
Water	Ponds, lakes, rivers, wetland and oceans	3.74%	Blue
Unknown	Clouds and other	0.04%	Black

the first public dataset that provides high-resolution submeter remote sensing images from rural areas [63]. This dataset contains a total of 1146 remote sensing images, which is divided into 75% training (803 images), 15% validation (171 images), and 15% test (172 images) sets. The size of each image is 2448×2448 pixels. All remote sensing images have a pixel resolution of 0.5 m and contain red-green-blue (RGB) color. Although the spectral information content of RGB images is not as high as that of multispectral images, the form of the final classification results generated from the RGB and multispectral images is the same; that is, different pixel blocks represent different land-use types, which will not affect the verification of the proposed SULR algorithm. The total area of these images is 1716.9 km^2 . Each image has a corresponding mask image of land cover classification

annotation. The land cover classification criteria come from the Anderson Classification [64], which contains seven classes that are marked with seven colors, as shown in Table I.

To test the proposed SULR method, we randomly selected remote sensing images of 100 regions. The corresponding mask images of land cover classification annotation are used as the input data. The total area of these regions is 149.82 km^2 . Fig. 7 shows some typical examples of selected remote sensing images and the corresponding preprocessing land cover classification results.

B. Results and Analysis

We generate land cover mapping results at two different levels using different parameter values. Figs. 8–10 show

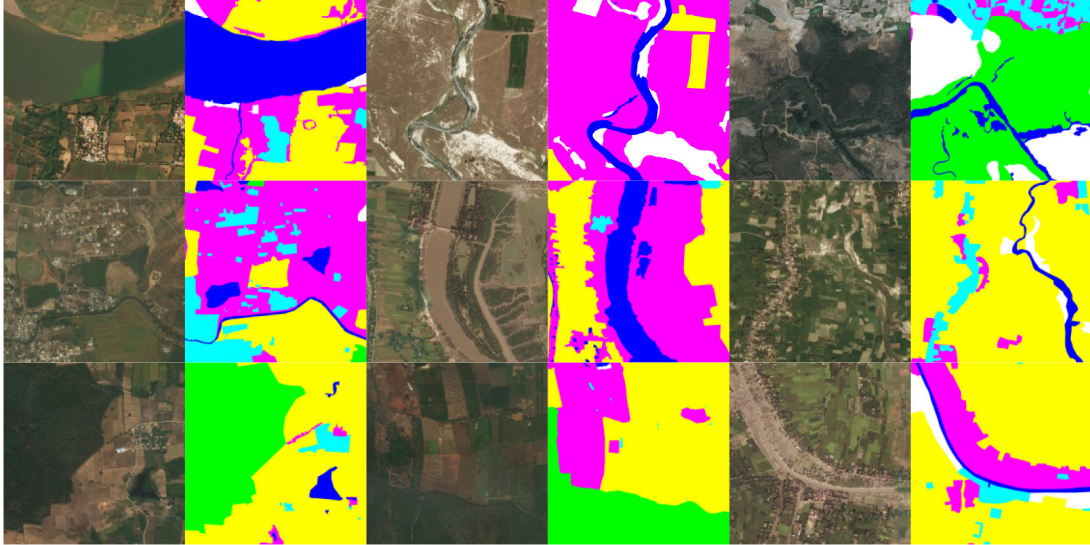


Fig. 7. Typical examples of land cover classification from remote sensing images.

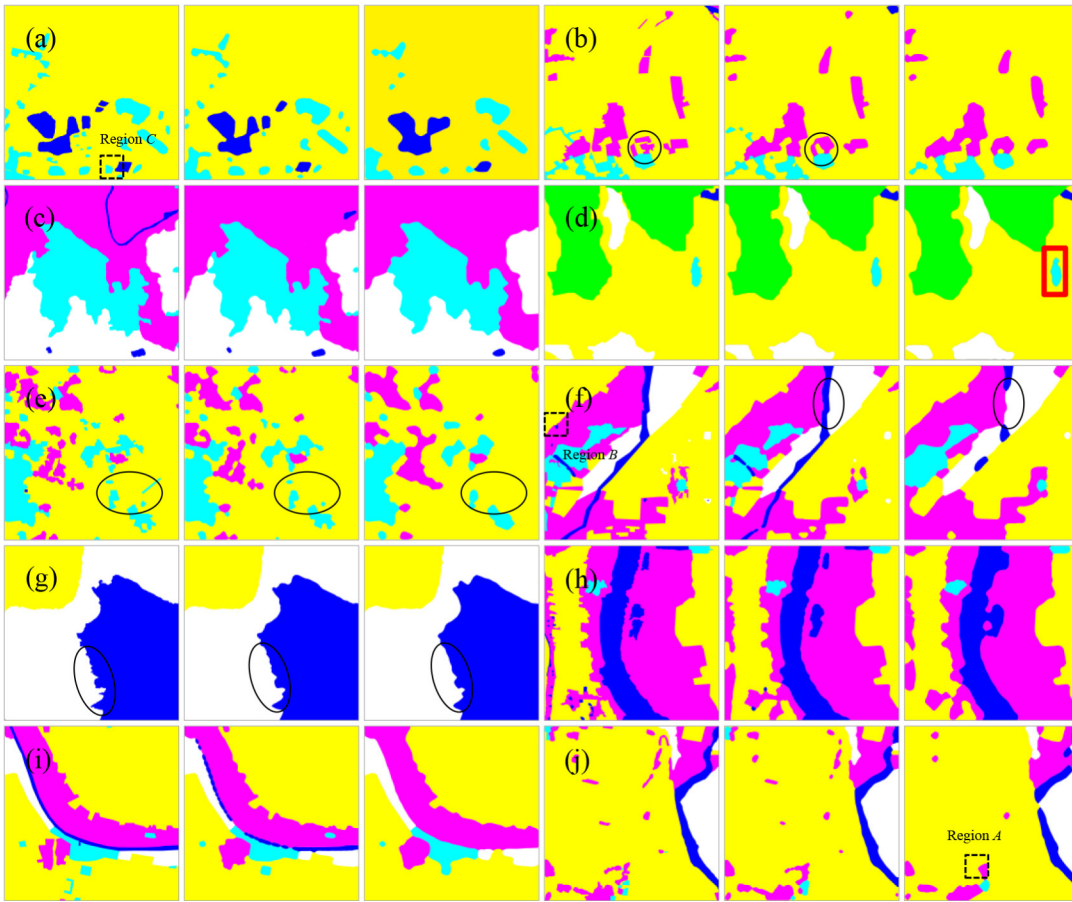


Fig. 8. Multiresolution mapping results using the proposed SULR method: part A. (a)–(j) Mapping results at two levels in different areas.

20 groups of typical multiresolution mapping results of land cover using the proposed SULR method. The LSC superpixel sizes used at these two levels are 30 and 60 pixels. In this process, as shown in Fig. 9, three special cases for LSC superpixel handling need to be emphasized as follows.

- 1) During aggregation, when an endpoint superpixel is totally surrounded by adjacent superpixels with the same semantic type, this endpoint superpixel should not be

subjected to a superpixel cutting operator. For example, in Fig. 9(a), the endpoint superpixel S_0 in Region A should not be performed by the superpixel cutting operator.

- 2) During amalgamation, when a signal superpixel detected by the superpixel cutting operator is totally surrounded by adjacent superpixels with different semantic types, this signal superpixel should be directly merged to the

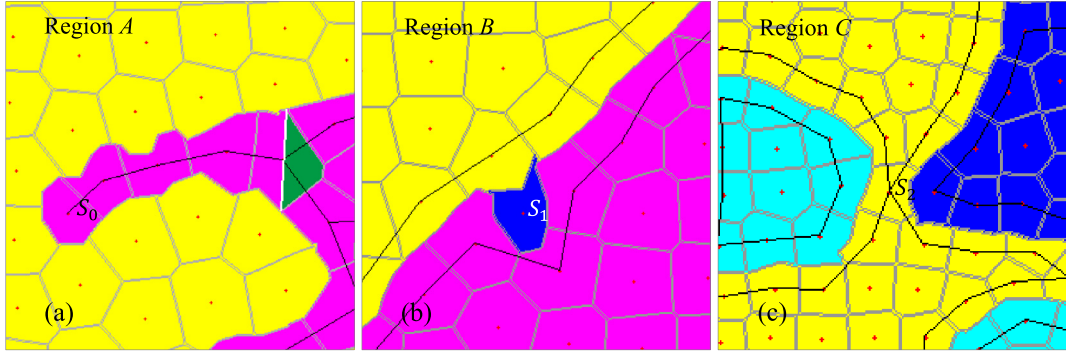


Fig. 9. Three special cases for handling LSC superpixels. (a) Region A. (b) Region B. (c) Region C.

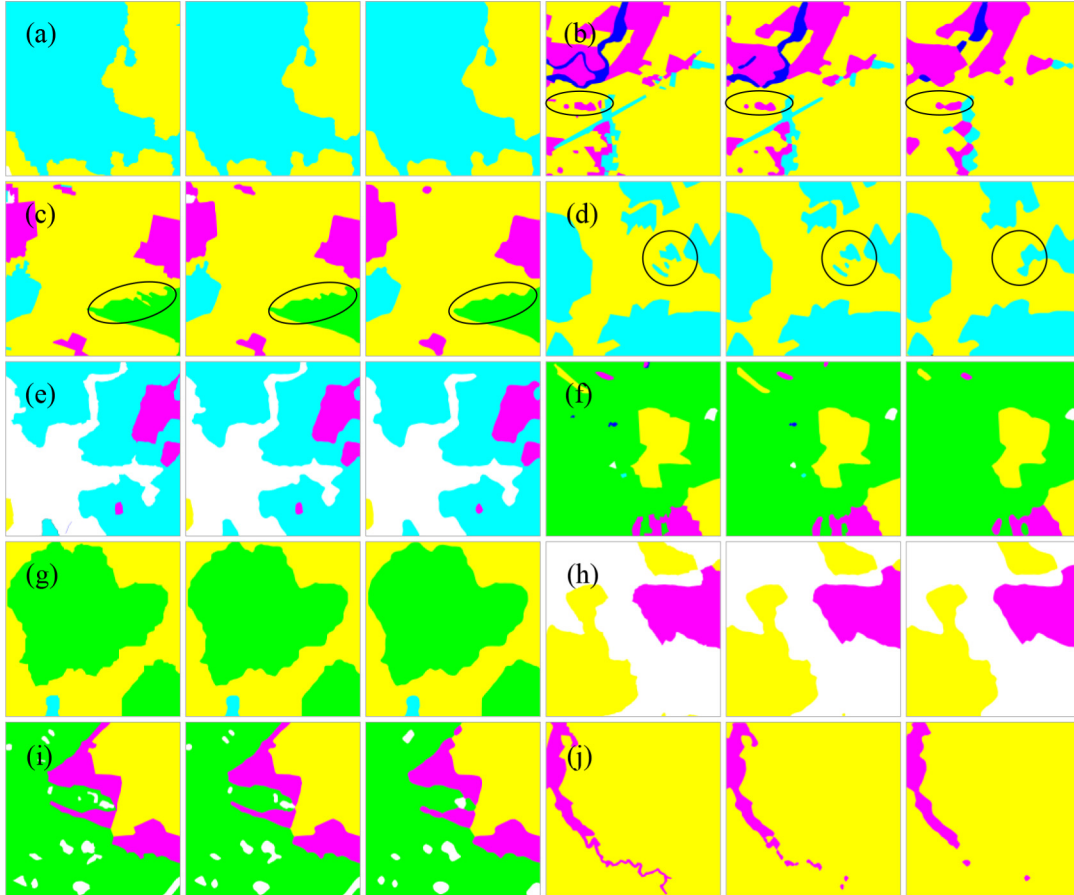


Fig. 10. Multiresolution mapping results using the proposed SULR method: part B. (a)–(j) Mapping results at two levels in different areas.

semantic type with the longest overlapping boundaries. For example, in Fig. 9(b), the signal blue superpixel S_1 is totally surrounded by the adjacent red and yellow superpixels, and the overlapping boundary with adjacent red superpixels is longer than that of the yellow superpixels. In this case, the signal blue superpixel S_1 should be directly merged with the red superpixels.

- 3) During amalgamation, when a signal superpixel detected by the superpixel cutting operator is not totally surrounded by adjacent superpixels with different semantic types, this signal superpixel should preserve the original state. For example, in Fig. 9(c), the signal yellow superpixel S_2 that connected the blue and Cyan superpixels should be preserved.

From the multiresolution mapping results of land cover in Figs. 8 and 10, several characteristics of the proposed SULR method can be observed. With an increasing mapping level, the boundaries of polygons can be smoothed, including the regions marked with ellipses in Figs. 8(g) and 10(c); the small land parcels can be removed, including the regions marked with ellipses in Figs. 8(e) and 10(b); the adjacent land parcels with short distances can be merged, including the regions marked with circles in Figs. 8(b) and 10(d); and the long and arrow land parcels can be uniformly divided into adjacent land parcels, including the regions marked with ellipses in Fig. 8(f).

To show the advantages of the proposed SULR method, we used traditional NNI, MF, and three deep learning-based methods to conduct contrast experiments. NNI is the simplest

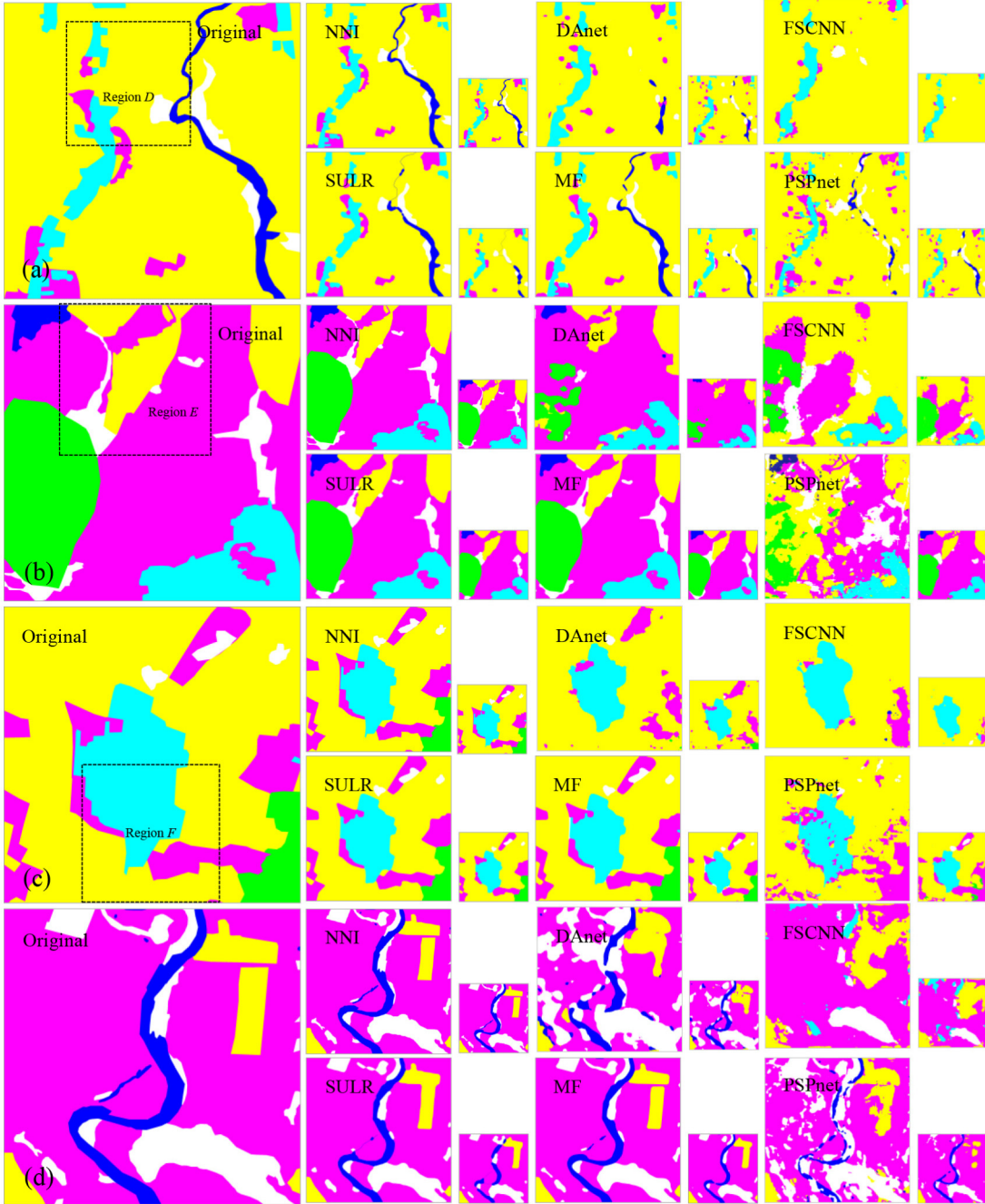


Fig. 11. Comparisons among the interpolation, filtering, and deep learning methods. (a)–(d) Mapping results at two levels in different areas.

technique for image scaling, in which the new pixel values are replaced with the pixel values from the nearest neighboring locations [14]. In the median filter technique, the median values of input samples are used to calculate the output samples using windows of various sizes [15]. The three deep learning-based methods used were DAnet [65], Fast-SCNN [66], and PSPnet [67].

Figs. 11 and 12 show comparisons of land cover mapping at two levels among the proposed SULR method, NNI, MF, and the three deep learning-based methods. The linear aperture sizes used in the MF method at the two levels are 61 and 121. In the three deep learning-based methods, to generate land cover mapping results at different resolutions, the original

training samples are reduced by a half (1224×1224 pixels) and a quarter (612×612 pixels) through the nearest sampling. The mIoU values of the DAnet, Fast-SCNN, and PSPnet models at the two levels are (0.78, 0.70), (0.53, 0.51), and (0.71, 0.68). The corresponding pixel accuracy values are (0.95, 0.92), (0.84, 0.82), and (0.93, 0.90). From Figs. 11 and 12, we can see the following characteristics.

- 1) *Geometric Characteristics:* The simplification of boundary geometric characteristics of land cover at different levels is helpful for providing better visual effects. Compared with the NNI method, the SULR and MF methods can effectively simplify the redundant details of the boundaries of land cover polygons, while the NNI

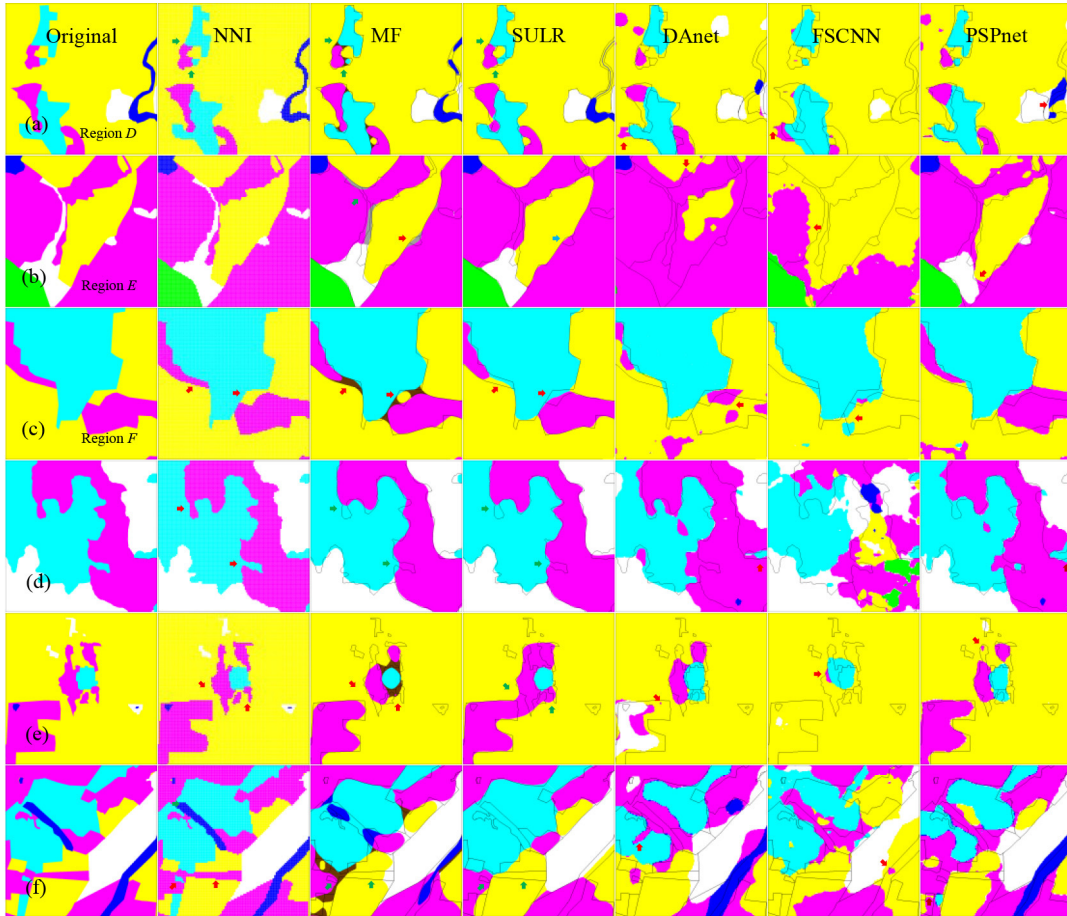


Fig. 12. Detailed comparisons of land cover multilevel mapping using the six methods. (a)–(f) Detailed mapping results in different areas.

method tends to generate jagged edges [such as the regions marked with red arrows in Fig. 12(d)]. During boundary simplification of the SULR and MF methods, the convex parts can be cut, and the concave parts can be filled, including the regions marked with green arrows in Fig. 12(d).

- 2) *Topologic Characteristics*: Topological relationships can clearly reflect the logical structure relations between land parcels, which greatly contribute to the spatial query. The MF method tends to break the original topologic relationship, especially in the adjacent areas of multiple land parcels with various semantic types. For example, as shown in the areas marked with red arrows in region D of Fig. 12(a), the original land parcels are topologically adjoining. After MF, some new pixel blocks are generated, and the adjoining land parcels become separated. However, the NNI and proposed SULR methods performed better at preserving the original topologic relationships of the adjacent areas of multiple land parcels, including the areas marked with green arrows in region D of Fig. 12(a).
- 3) *Semantic Characteristics*: The reasonable combination and uniform division of land cover with different semantic characteristics can help to preserve the relative percentage of land parcel areas. The proposed SULR

method can reasonably merge land parcels of the same semantic types that are short distances apart, while the NNI method cannot, including the regions marked with arrows in Fig. 12(e). Although the MF can sometimes merge land parcels [such as the regions marked with green arrows in Fig. 12(b)], in most cases, it cannot realize a combination of small land parcels [such as the regions marked with red arrows in Fig. 12(e)]. For some small land parcels surrounded by multiple land parcels with different semantic types, the proposed SULR method can uniformly divide the long and narrow land parcels into adjacent land parcels with various semantic types, including the areas marked with green arrows in region F of Fig. 12(c). However, the MF tends to generate new long and narrow land parcels with different colors, and the NNI method cannot realize uniform division, including the areas marked with red arrows in region F of Fig. 12(c).

- 4) *Minimum Visible Characteristics*: With the shrinkage of the land cover map, visually illegible land parcels with small sizes should be removed to avoid a reading burden. The proposed SULR method can optionally transfer areal land parcels with long and narrow shapes to corresponding linear features, such as the blue rivers in Fig. 12(a). This method can also effectively remove the land parcels with small areas, such as the regions

TABLE II
AVERAGE VALUES OF AREA CHANGES

Methods		Agriculture	Forest	Rangeland	Urban	Barren	Water
		Land	Land	Land	Land	Land	
Level 01	MF	5349.73	3385.64	-343.28	-5367.73	2137.65	-5162.01
	SULR	5287.71	3073.20	-312.64	-5293.63	2724.38	-5479.02
	DAnet	64474.11	-14301.98	-67858.64	-29783.05	83641.51	-32742.16
	FSCNN	301340.67	-27146.97	-379833.39	-63875.19	183264.47	-11786.19
Level 02	PSPnet	-22272.62	-1378.67	-18439.28	-23383.16	68754.75	-3405.15
	MF	23729.74	12174.71	-7027.18	-17089.28	5275.76	-17063.75
	SULR	21395.26	11694.08	-3854.10	-13862.38	4063.85	-19436.71
	DAnet	134835.12	86054.89	-141666.04	-100580.47	36255.77	-6885.88
	FSCNN	649714.42	-22326.99	-203426.04	-93610.70	-335495.67	-260.89
	PSPnet	313783.59	30392.10	-167465.54	-126880.16	-112108.55	55507.08

marked with green arrows in Fig. 12(b) and (f). Although the MF can sometimes remove land parcels with small sizes [such as the regions marked with green arrows in Fig. 12(f)], in some cases, it may transform the small land parcels to long and narrow shapes [such as the regions marked with red arrows in Fig. 12(b)]. In most cases, the NNI method cannot remove land parcels with small sizes, such as the regions marked with red arrows in Fig. 12(f).

Due to the uncontrollability of the generated results, the three deep learning-based methods (DAnet, Fast-SCNN, and PSPnet) perform poorly in these four aspects of geometric, topologic, semantic, and minimum visible characteristics. For example, in Fig. 12(a) and (b), the geometric boundaries marked with red arrows are very rough; in Fig. 12(c), the topologic relationships of the adjacent land parcels marked with red arrows are broken; in Fig. 12(d), the reasonable combination and uniform division of land parcels marked with red arrows with different semantic characteristics are not realized; and in Fig. 12(e) and (f), visually illegible land parcels with small sizes are not effectively removed.

To quantitatively evaluate the proposed SULR method, we calculate the geometric changes in the area, perimeter, and location accuracies of land cover boundaries based on areal displacement [68].

Fig. 13 and Table II present the area changes of six types of land parcels, namely agricultural land, forestland, rangeland, urban land, barren land, and water, at two levels using the MF, SULR, and deep learning methods, from which we can identify the following characteristics.

- With an increasing mapping level, the area changes in six types of land cover generated from the MF, SULR, and deep learning (DAnet, Fast-SCNN, and PSPnet) methods basically increase.
- For most of the land cover types at two levels, the area change values generated from the SULR method are lower than those of the MF and deep learning (DAnet, Fast-SCNN, and PSPnet) methods. For example, at level 1, the area changes in agricultural land, forestland,

rangeland, and urban land (marked with bold fonts in Table II) generated from the proposed SULR method are lower than those of the MF and deep learning methods. At level 2, the area changes in agricultural land, forestland, rangeland, urban land, and barren land (marked with bold fonts in Table II) generated from the proposed SULR method are lower than those of the MF and deep learning methods. Conversely, the area change in water generated from the proposed SULR method is higher than that of the MF method, which is because most of the water is composed of long and narrow rivers in the experimental areas, and these rivers collapse to linear features when using the proposed SULR method.

- During the deep learning methods, the area change values of the land cover types at two levels generated from the DAnet and PSPnet methods are significantly lower than those of the FSCNN method.

Fig. 14 and Table III show the perimeter changes in six types of land parcels at two levels using the MF, SULR, and deep learning methods, from which we can identify the following characteristics.

- With increasing mapping level, the perimeter changes in six types of land cover generated from the MF, SULR, and deep learning methods basically increase.
- The land cover types with maximal perimeter changes in the MF method at levels 1 and 2 are both rangeland. The land cover types with maximal perimeter changes in the SULR method at levels 1 and 2 are also rangeland, while the land cover types with maximal perimeter changes in the deep learning methods at levels 1 and 2 are not fixed.
- The average perimeter changes generated from the SULR method are higher than those from the MF method but lower than those from the deep learning methods at level 1. At level 2, the average perimeter change generated from the DAnet is the lowest, while the other two deep learning methods perform poorly.

Fig. 15 shows the areal displacement of land parcels at two levels using the MF, SULR, and deep learning methods. The areal displacement of two polygons can be acquired

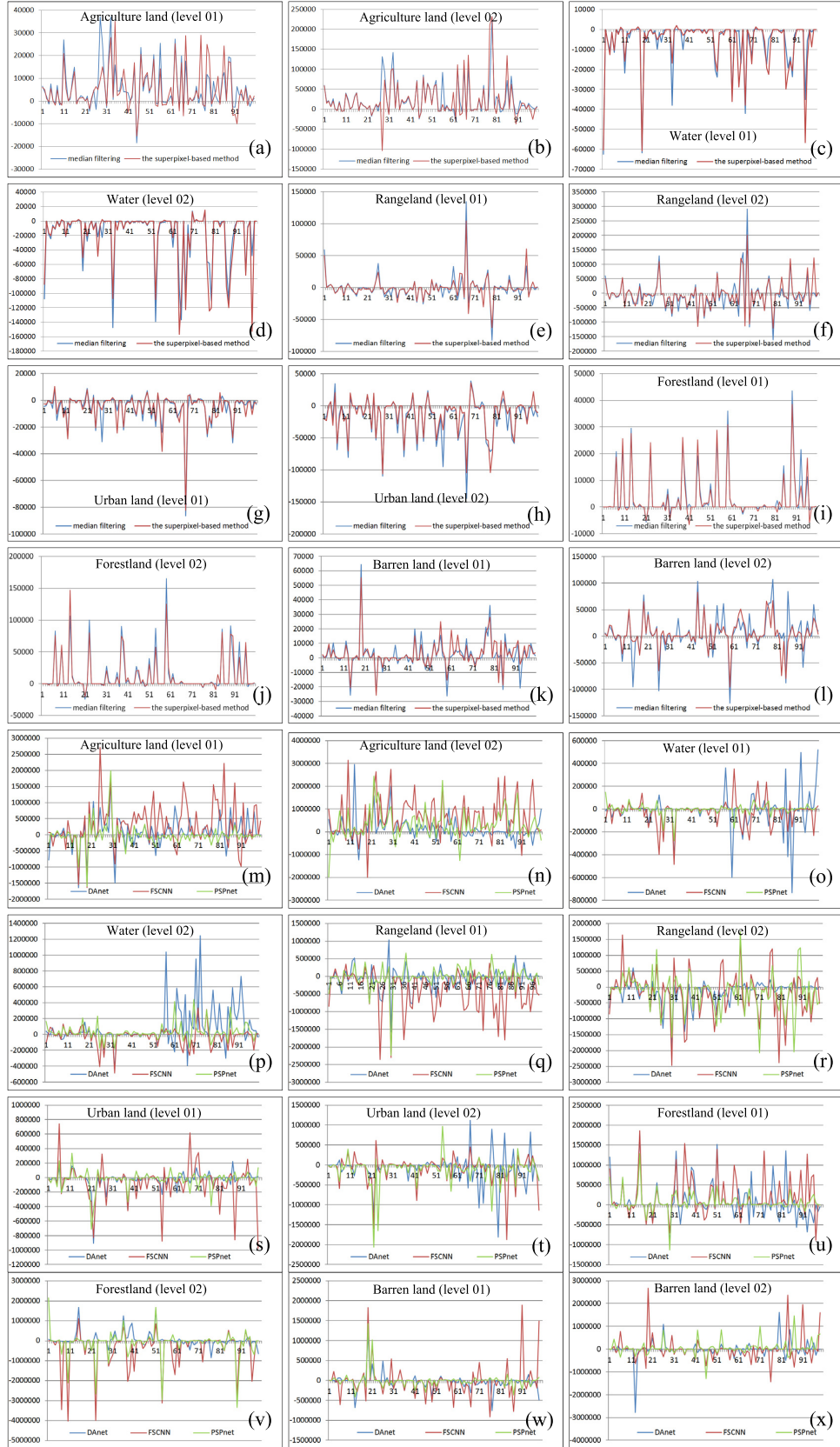


Fig. 13. Area changes in land parcels at two levels using the MF, SULR, and deep learning methods. Area changes at two levels using (a)-(l) MF and SULR methods and (m)-(x) deep learning methods.

by calculating the area values of the nonoverlapping parts, which is used to measure the location accuracy boundaries during simplification [68]. At these two levels, the average

areal displacements of MF (60 568.57 at level 1 and 173 122.19 at level 2) are both lower than the average areal displacement of the proposed SULR method (67 214.21 at

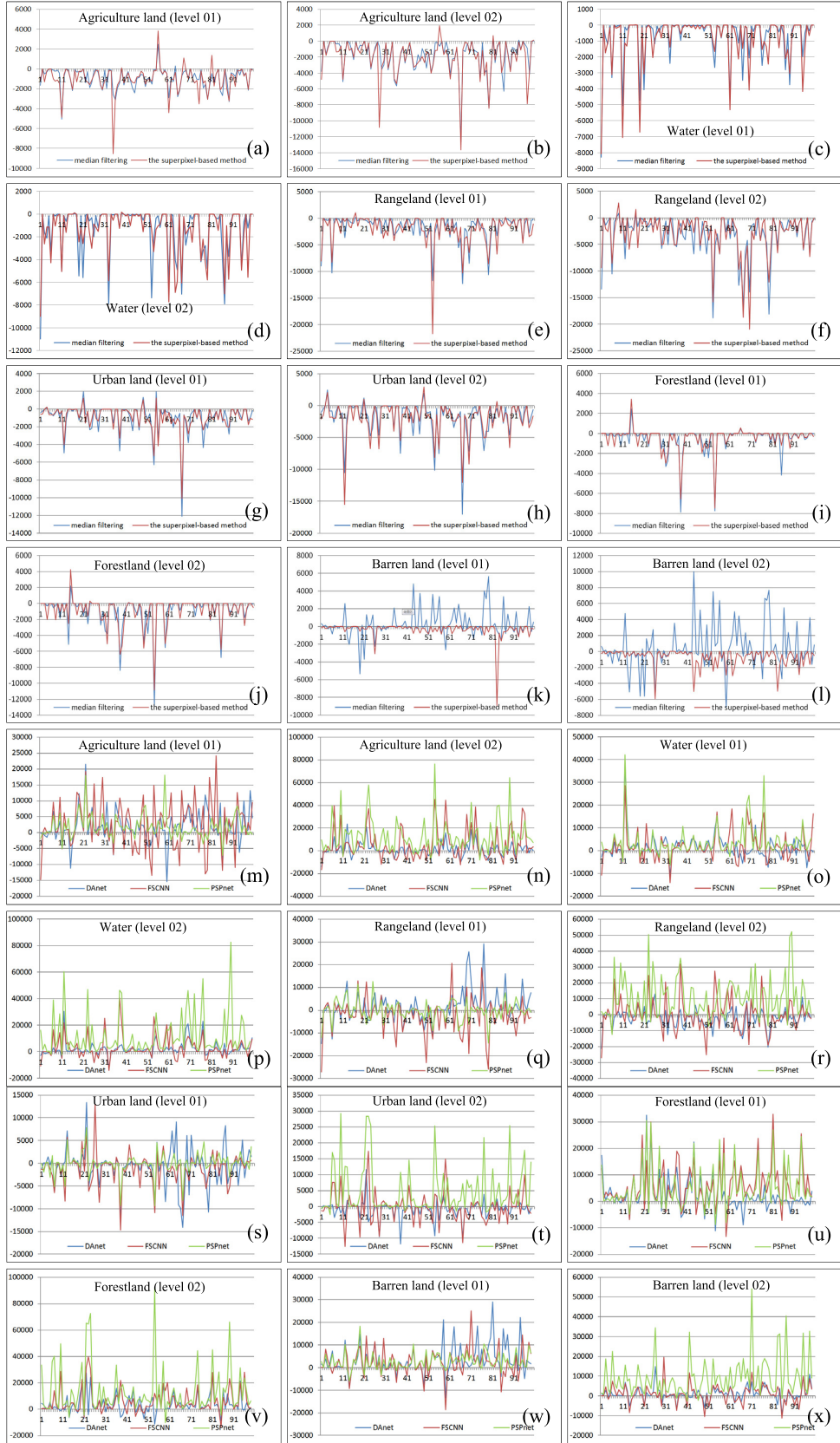


Fig. 14. Perimeter changes in land parcels at two levels using the MF, SULR, and deep learning methods. Perimeter changes at two levels using (a)–(l) MF and SULR methods and (m)–(x) deep learning methods.

level 1 and 180 184.27 at level 2). The main reasons that produce the geometric and positional differences between the MF and SULR methods are because the SULR method can

merge the adjacent land parcels, divide (collapse) the long and narrow land parcels, and remove the small land parcels in the area. The areal displacements generated by each of the DAnet

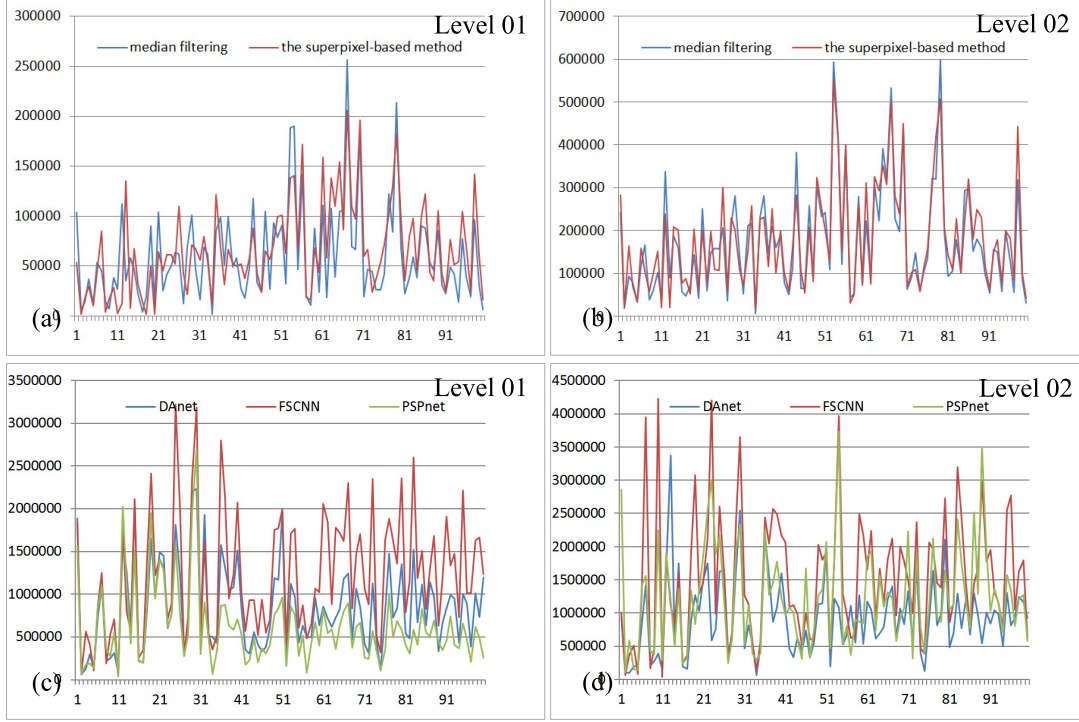


Fig. 15. Areal displacement of land parcels at two levels using the MF, SULR, and deep learning methods. Areal displacement of (a) MF and SULR at level 1, (b) MF and SULR at level 2, (c) deep learning methods at level 1, and (d) deep learning methods at level 2.

TABLE III
AVERAGE VALUES OF PERIMETER CHANGES

Methods		Agriculture land	Forest land	Rangeland	Urban land	Barren land	Water	Average perimeter change
Level 01	MF	-897.92	-493.66	-1731.40	-903.51	259.98	-672.66	-739.86
	SULR	-991.57	-467.18	-2033.18	-922.45	-359.52	-824.33	-933.04
	DAnet	1894.95	1504.86	1765.07	-651.43	2674.35	3418.23	1767.67
	FSCNN	2471.95	2027.43	-2292.21	-1089.51	6017.66	2213.86	1558.20
	PSPnet	1843.54	3772.53	-114.19	-59.52	4976.67	2762.27	2196.88
Level 02	MF	-1794.71	-895.14	-3079.00	-1752.53	435.65	-1285.15	-1395.15
	SULR	-2011.27	-897.37	-2924.37	-1933.50	-726.74	-1397.88	-1648.52
	DAnet	1321.43	2185.42	-2144.34	-870.38	3973.00	1048.27	918.9
	FSCNN	5452.15	3195.09	-216.74	-141.53	6118.61	992.94	2566.75
	PSPnet	12802.36	11844.37	10866.29	4707.91	13853.26	9366.51	10573.45

(844 800.62 at level 1 and 931 562.07 at level 2), Fast-SCNN (1 239 041.27 at level 1 and 1 530 258.53 at level 2), and PSPnet (624 591.53 at level 1 and 1 226 457.49 at level 2) methods are higher than that generated by the MF and SULR methods, which indicates that deep learning methods can cause larger shape changes.

C. Application to Multispectral Images of Tianjin City

We used multispectral Landsat ETM+ images with a resolution of 30 m from Tianjin city in China to test the proposed SULR method. As shown in Fig. 16(a), the north latitude and east longitude ranges of the remote sensing images of Tianjin

city displayed are $38^{\circ}34' < \text{lat} < 40^{\circ}15'$ and $116^{\circ}43' < \text{lon} < 118^{\circ}19'$. The results of overlay displaying of selected RGB bands are shown in Fig. 16(b). Tianjin has a total land area of 1.1919 million hectares. Within this area, the cultivated area is 445 500 ha, accounting for 37.4% of the total land area of the city. Residential land and industrial and mining land occupy 262 500 ha, and the unused land area is 138 200 ha. After band selection and fusion, geometric correction and registration of the images, and image enhancement, mosaic and clipping, the land-use types in Tianjin were divided into 25 categories [69] based on manual and visual interpretation, which achieved an accuracy rate of 98.15%. The original results of land cover classification from the Landsat ETM+ images in Tianjin can

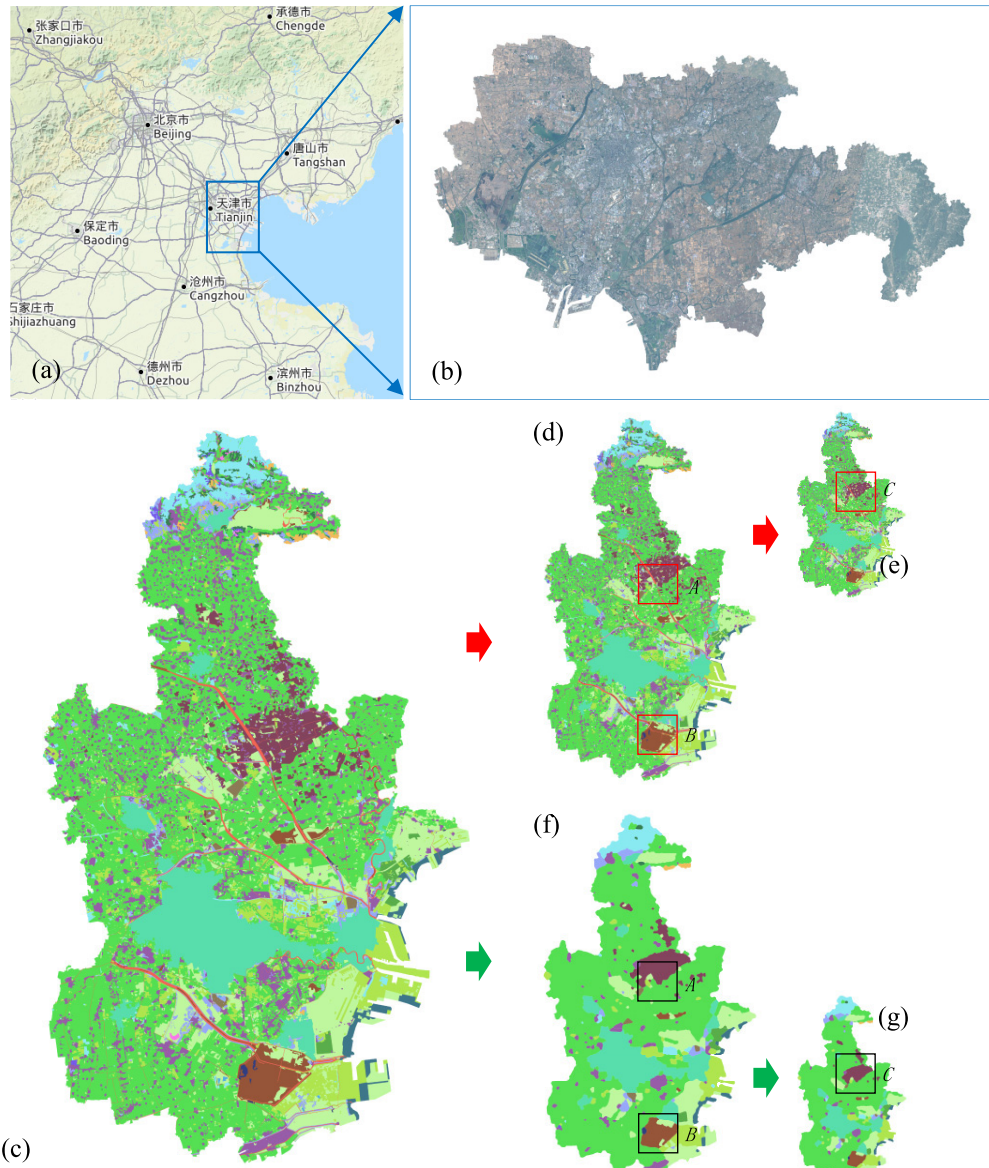


Fig. 16. Multiresolution mapping of land cover in Tianjin from Landsat ETM+ images using the SULR method. (a) Geographic range of Tianjin. (b) Original remote sensing images. (c) Land cover classification. (d) and (e) Multiresolution mapping using traditional scaling method. (f) and (g) Multiresolution mapping using the SULR method.

be found in Fig. 16(c). The mapping results of land cover generated using the proposed SULR method at two different levels of detail in Tianjin city can be found in Fig. 16(e) and (f). The LSC superpixel sizes used at these two levels were 80 and 120 pixels.

The geometric changes in the area and length of all land cover types at the two different levels are shown in Fig. 17. At level 1, as shown in Fig. 17(a) and (c), large changes in the area of land cover are evident; the maximum area change of all land-use types is 1 978 635, which accounts for 28.4% of the total area. This change is mainly due to the aggregation of a large number of tiny land parcels. At level 2, as shown in Fig. 17(b) and (d), there are small changes in the area of land cover; the maximum area change of all land-use types is 285 116, which accounts for only 3.1% of the total area. This result is due mainly to the effect of boundary simplification. Similarly, at level 1, due to a large number of merged small

patches, the length greatly changed. As shown in Fig. 17(e) and (g), the maximum length change of all land-use types is 226 087, which accounts for 80.7% of the total length. At level 2, due to the influence of boundary simplification, the change in length is small. As shown in Fig. 17(f) and (h), the maximum length change of all land-use types is 9300, which accounts for 51.3% of the total length. From level 1 to level 2, the number of visible land-use types decreases from 5 to 6. The percentages of areal displacement to the total area of land parcels at the two levels using the SULR method are 0.259 and 0.287. Compared with the traditional scaling method [Fig. 16(d) and (e)], the proposed SULR method performs better in the following aspects. First, using the SULR method, long and narrow land parcels can be uniformly integrated into multiple other types of adjacent land parcels, whereas the traditional scaling method cannot realize this integration. For example, in region A, using the proposed SULR method,

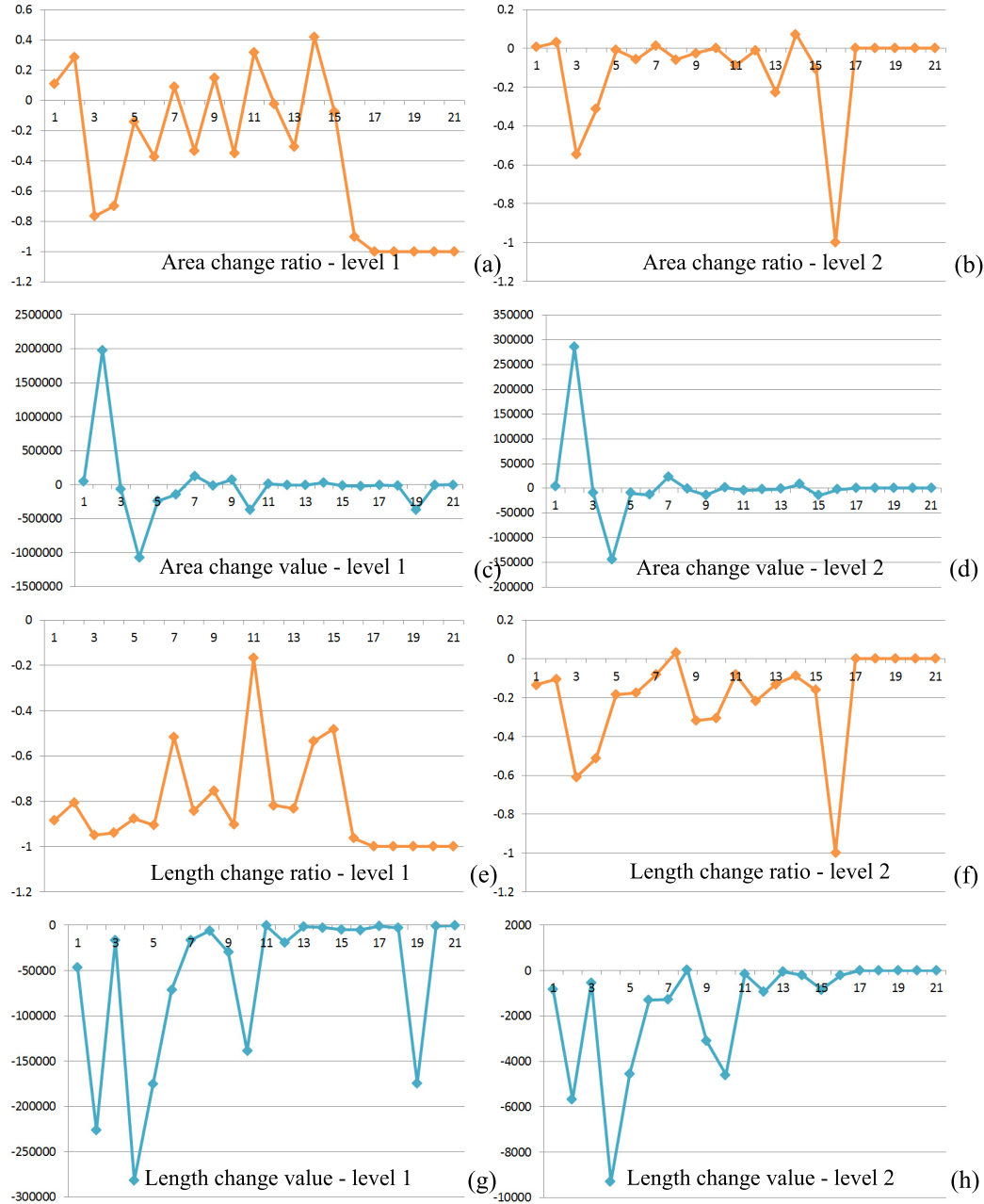


Fig. 17. Geometric changes in the area and perimeter of Tianjin land cover at two different levels. (a) Area change ratio at level 1. (b) Area change ratio at level 2. (c) Area change value at level 1. (d) Area change value at level 2. (e) Length change ratio at level 1. (f) Length change ratio at level 2. (g) Length change value at level 1. (h) Length change value at level 2.

the orange land parcels are merged into the brown and green land parcels. Second, the SULR method performs better in smoothing the boundaries of land cover, as evident in the polygonal boundaries of land cover in region *B*. Third, the tiny land parcels with small areas can be well removed using the proposed SULR method, which can provide a better visual effect than the traditional scaling method when reading the land cover map, as evident for the land parcels in region *C*.

V. CONCLUSION

Multiple constraint criteria, including topological, geometrical, and semantic characteristics, play important roles during multiresolution land cover mapping from remote sensing images. Traditional image scaling methods cannot consider these representation characteristics. In this study,

a superpixel-based method for multiresolution land cover mapping from remote sensing images (the SULR method) based on aggregation, amalgamation, and simplification operations was developed. In this process, three types of superpixel operations, namely collapse, connection, and cutting, are first defined. Based on three types of superpixel operations, the aggregation, amalgamation, and simplification of land cover are sequentially performed. Compared with traditional image processing methods, we obtain the following conclusions.

- 1) Compared with the interpolation method for image scaling, the proposed SULR method can effectively remove the redundant details of land cover boundaries by cutting the convex parts and filling the concave parts, which can avoid cognitive burdens for readers.

- 2) In contrast to the MF method for image smoothing, the proposed SULR method can effectively merge the adjacent land parcels with homogeneous semantics, divide (collapse) the long and narrow land parcels with heterogeneous semantics, and remove the small land parcels in the area, which enables better consideration of the topological and semantic characteristics during multiresolution land cover mapping.
- 3) Compared with the deep learning methods, the proposed SULR can better avoid the noise of tiny land parcels and produce smoother and more regular boundaries of land cover with higher mapping accuracy. In addition, the deep learning methods cannot consider the topological and semantic characteristics, whereas the proposed SULR can.

However, the limitations of this study should be addressed. First, the simplification of land cover types with orthogonal characteristics, such as buildings, is not considered in this study and should be further researched in the future. Second, during the aggregation of land parcels, whether or not the sum of changes in land parcels has been minimized with optimal solutions should be further studied.

REFERENCES

- [1] R. Mathieu, C. Freeman, and J. Aryal, "Mapping private gardens in urban areas using object-oriented techniques and very high-resolution satellite imagery," *Landscape Urban Planning*, vol. 81, no. 3, pp. 179–192, Jun. 2007.
- [2] J. P. Ardila, V. A. Tolpekin, W. Bijkér, and A. Stein, "Markov random field-based superresolution mapping for identification of urban trees in vhr images," *ISPRS J. Photogramm. Remote Sens.*, vol. 66, no. 6, pp. 762–775, 2011.
- [3] C. Zhang and J. M. Kovacs, "The application of small unmanned aerial systems for precision agriculture: A review," *Precis. Agricult.*, vol. 13, no. 6, pp. 693–712, Dec. 2012.
- [4] H. Shi, L. Chen, F.-k. Bi, H. Chen, and Y. Yu, "Accurate urban area detection in remote sensing images," *IEEE Geosci. Remote Sens. Lett.*, vol. 12, no. 9, pp. 1948–1952, Sep. 2015.
- [5] A. Ozdarici-Ok, A. Ok, and K. Schindler, "Mapping of agricultural crops from single high-resolution multispectral images—Data-driven smoothing vs. Parcel-based smoothing," *Remote Sens.*, vol. 7, no. 5, pp. 5611–5638, May 2015.
- [6] X.-Y. Tong *et al.*, "Land-cover classification with high-resolution remote sensing images using transferable deep models," *Remote Sens. Environ.*, vol. 237, Feb. 2020, Art. no. 111322.
- [7] D. A. Quattrochi and M. F. Goodchild, Eds., *Scale in Remote Sensing and GIS*. Boca Raton, FL, USA: CRC Press, 1997.
- [8] Q. Weng, Ed., *Scale Issues in Remote Sensing*. Hoboken, NJ, USA: Wiley, 2014.
- [9] J.-H. Haunert and A. Wolff, "Generalization of land cover maps by mixed integer programming," in *Proc. 14th Annu. ACM Int. Symp. Adv. Geographic Inf. Syst. (GIS)*, 2006, pp. 75–82.
- [10] K. S. Shea and R. B. M. Master, "Cartographic generalization in a digital environment," in *Proc. Auto-Carto*, vol. 9, 1989, p. 5667.
- [11] T. Cheng and Z. Li, "Toward quantitative measures for the semantic quality of polygon generalization," *Cartographica*, vol. 41, no. 2, pp. 487–499, 2006.
- [12] S. Steiniger and R. Weibel, "Relations among map objects in cartographic generalization," *Cartography Geographic Inf. Sci.*, vol. 34, no. 3, pp. 175–197, Jan. 2007.
- [13] J.-H. Haunert and A. Wolff, "Area aggregation in map generalisation by mixed-integer programming," *Int. J. Geograph. Inf. Sci.*, vol. 24, no. 12, pp. 1871–1897, Nov. 2010.
- [14] L. Tan and J. Jiang, *Digital Signal Processing: Fundamentals and Applications*. Amsterdam, The Netherlands: Elsevier, 2007.
- [15] L. Deligiannidis and H. Arabnia, *Emerging Trends in Image Processing Computer Vision and Pattern Recognition*. San Mateo, CA, USA: Morgan Kaufmann, 2014.
- [16] T. Ai and Y. Liu, "Aggregation and amalgamation in land-use data generalization," *Geomatics Inf. Sci. Wuhan Univ.*, vol. 27, no. 5, pp. 486–492, 2002.
- [17] Q. Guo, X. Wang, and J. Liu, "Progressive combination of polygon groups," *Geomatics Inf. Sci. Wuhan Univ.*, vol. 37, no. 2, pp. 220–223, 2012.
- [18] M. Cacciola, F. C. Morabito, and G. Simone, *Image Fusion: Algorithms and Applications*. New York, NY, USA: Academic, 2008.
- [19] M. G. Madan, "Soft computing and intelligent systems," *Kybernetes*, vol. 30, no. 1, pp. 23–38, 2014.
- [20] C. Arcelli and G. Ramella, "Finding contour-based abstractions of planar patterns," *Pattern Recognit.*, vol. 26, no. 10, pp. 1563–1577, Oct. 1993.
- [21] M. Marji and P. Siy, "Polygonal representation of digital planar curves through dominant point detection—A nonparametric algorithm," *Pattern Recognit.*, vol. 37, no. 11, pp. 2113–2130, Nov. 2004.
- [22] P. Bhowmick and B. B. Bhattacharya, "Fast polygonal approximation of digital curves using relaxed straightness properties," *IEEE Trans. Pattern Anal. Mach. Intell.*, vol. 29, no. 9, pp. 1590–1602, Sep. 2007.
- [23] B. Cheng, Q. Liu, X. Li, and Y. Wang, "Building simplification using backpropagation neural networks: A combination of cartographers' expertise and raster-based local perception," *GISci. Remote Sens.*, vol. 50, no. 5, pp. 527–542, Oct. 2013.
- [24] Y. Shen, T. Ai, and Y. He, "A new approach to line simplification based on image processing: A case study of water area boundaries," *ISPRS Int. J. Geo-Inf.*, vol. 7, no. 2, p. 41, Jan. 2018.
- [25] Y. Shen, T. Ai, and C. Li, "A simplification of urban buildings to preserve geometric properties using superpixel segmentation," *Int. J. Appl. Earth Observ. Geoinf.*, vol. 79, pp. 162–174, Jul. 2019.
- [26] Y. Shen, T. Ai, W. Li, M. Yang, and Y. Feng, "A polygon aggregation method with global feature preservation using superpixel segmentation," *Comput. Environ. Urban Syst.*, vol. 75, pp. 117–131, May 2019.
- [27] L. Schylberg, "Computational methods for generalisation of cartographic data in a raster environment," Ph.D. dissertation, Dept. Geodesy Photogramm., Royal Institute of Technology, Stockholm, Sweden, 1993.
- [28] B. Su, Z. Li, G. Lodwick, and J.-C. Muller, "Algebraic models for the aggregation of area features based upon morphological operators," *Int. J. Geograph. Inf. Sci.*, vol. 11, no. 3, pp. 233–246, Apr. 1997.
- [29] M. Cámera and F. López, "Mathematical morphology applied to raster generalization of urban city block maps," *Cartographica, Int. J. Geographic Inf. Geovisualization*, vol. 37, no. 1, pp. 33–48, Mar. 2000.
- [30] A. Boffet and S. R. Serra, "Identification of spatial structures within urban blocks for town characterisation," in *Proc. 20th Int. Cartographic Conf. (ICC)*, vol. 3, Beijing, China, Aug. 2001, pp. 1974–1983.
- [31] P. J. M. van Oosterom, "The GAP-tree, an approach to 'on-the-fly' map generalization of an area partitioning," in *GIS and Generalization -Methodology and Practice*, J.C. Müller, J. P. Lagrange, and R. Weibel, Eds. London, U.K.: Taylor & Francis, 1995.
- [32] N. Regnault, "Algorithms for the amalgamation of topographic data," in *Proc. 21st Int. Cartographic Conf. (CD-ROM)*, 2003, pp. 222–233.
- [33] T. Lang, "Rules for the robot draughtsmen," *Geograph. Mag.*, vol. 42, no. 1, pp. 50–51, 1969.
- [34] D. H. Douglas and T. K. Peucker, "Algorithms for the reduction of the number of points required to represent a digitized line or its caricature," *Cartographica, Int. J. Geographic Inf. Geovisualization*, vol. 10, no. 2, pp. 112–122, Dec. 1973.
- [35] Z. Li and S. Openshaw, "Algorithms for automated line generalization based on a natural principle of objective generalization," *Int. J. geographical Inf. Syst.*, vol. 6, no. 5, pp. 373–389, Sep. 1992.
- [36] M. Visvalingam and J. D. Whyatt, "Line generalization by repeated elimination of points," *Cartographic J.*, vol. 30, no. 1, pp. 46–51, 1993.
- [37] N. Mustafa, S. Krishnan, G. Varadhan, and S. Venkatasubramanian, "Dynamic simplification and visualization of large maps," *Int. J. Geograph. Inf. Sci.*, vol. 20, no. 3, pp. 273–302, Mar. 2006.
- [38] M. Nöllenburg, D. Merrick, A. Wolff, and M. Benkert, "Morphing polylines: A step towards continuous generalization," *Comput. Environ. Urban Syst.*, vol. 32, no. 4, pp. 248–260, Jul. 2008.
- [39] P. Raposo, "Scale-specific automated line simplification by vertex clustering on a hexagonal tessellation," *Cartography Geographic Inf. Sci.*, vol. 40, no. 5, pp. 427–443, Nov. 2013.
- [40] T. Gökgöz, "A new algorithm for cartographic simplification of streams and lakes using deviation angles and error bands," *ISPRS Int. J. Geo-Inf.*, vol. 4, no. 4, pp. 2185–2204, 2015.
- [41] S. de Bruin, "Modelling positional uncertainty of line features by accounting for stochastic deviations from straight line segments," *Trans. GIS*, vol. 12, no. 2, pp. 165–177, Apr. 2008.

- [42] C. Dyken, M. Dæhlen, and T. Sevaldrud, "Simultaneous curve simplification," *J. Geograph. Syst.*, vol. 11, no. 3, pp. 273–289, Sep. 2009.
- [43] A. Saalfeld, "Topologically consistent line simplification with the Douglas-Peucker algorithm," *Cartography Geographic Inf. Sci.*, vol. 26, no. 1, pp. 7–18, Jan. 1999.
- [44] K. Buchin, W. Meulemans, A. Renssen, and B. Speckmann, "Area-preserving simplification and schematization of polygonal subdivisions," *ACM Trans. Spatial Algorithms Syst.*, vol. 2, no. 1, pp. 1–35, 2016.
- [45] W. Xu, Y. Long, T. Zhou, and L. Chen, "Simplification of building polygon based on adjacent four-point method," *Acta Geodaetica et Cartographica Sinica*, vol. 42, no. 6, pp. 929–936, 2013.
- [46] M. Sester, "Generalization based on least squares adjustment," in *Proc. Int. Arch. Photogramm.*, 2000, pp. 931–938.
- [47] Y. Zhang, X. Sun, H. Wang, and K. Fu, "High-resolution remote-sensing image classification via an approximate Earth mover's distance-based bag-of-features model," *IEEE Geosci. Remote Sens. Lett.*, vol. 10, no. 5, pp. 1055–1059, Sep. 2013.
- [48] S. Chen and Y. Tian, "Pyramid of spatial relations for scene-level land use classification," *IEEE Trans. Geosci. Remote Sens.*, vol. 53, no. 4, pp. 1947–1957, Apr. 2015.
- [49] M. Castelluccio, G. Poggi, C. Sansone, and L. Verdoliva, "Land use classification in remote sensing images by convolutional neural networks," 2015, *arXiv:1508.00092*. [Online]. Available: <http://arxiv.org/abs/1508.00092>
- [50] X. Ren and J. Malik, "Learning a classification model for segmentation," in *Proc. 9th IEEE Int. Conf. Comput. Vis.*, Oct. 2003, p. 10.
- [51] Z. Li and J. Chen, "Superpixel segmentation using linear spectral clustering," in *Proc. IEEE Conf. Comput. Vis. Pattern Recognit. (CVPR)*, Jun. 2015, pp. 1356–1363.
- [52] T. Ai and P. van Oosterom, "A map generalization model based on algebra mapping transformation," in *Proc. 9th ACM Int. Symp. Adv. Geographic Inf. Syst. (GIS)*, 2001, pp. 21–27.
- [53] A. Rosenfeld and E. Johnston, "Angle detection on digital curves," *IEEE Trans. Comput.*, vol. C-22, no. 9, pp. 875–878, Sep. 1973.
- [54] L. Kitchen and A. Rosenfeld, "Gray-level corner detection," *Pattern Recognit. Lett.*, vol. 1, no. 2, pp. 95–102, Dec. 1982.
- [55] C. Harris and M. Stephens, "A combined corner and edge detector," in *Proc. Alvey Vis. Conf.*, 1988, pp. 147–151.
- [56] H.-C. Liu and M. D. Srinath, "Corner detection from chain-code," *Pattern Recognit.*, vol. 23, nos. 1–2, pp. 51–68, Jan. 1990.
- [57] S. M. Smith and J. M. Brady, "SUSAN—A new approach to low-level image processing," *Int. J. Comput. Vis.*, vol. 23, no. 1, pp. 45–78, 1997.
- [58] F. Chabat, G. Z. Yang, and D. M. Hansell, "A corner orientation detector," *Image Vis. Comput.*, vol. 17, no. 10, pp. 761–769, Aug. 1999.
- [59] J. Shi and Tomasi, "Good features to track," in *Proc. IEEE Conf. Comput. Vis. Pattern Recognit. (CVPR)*, Jun. 1994, pp. 593–600.
- [60] J.-Y. Bouguet, *Pyramidal Implementation of the Lucas Kanade Feature Tracker, Description of the Algorithm*. Santa Clara, CA, USA: Intel Corporation, 2000.
- [61] A. Kolesnikov and P. Fräntti, "Polygonal approximation of closed discrete curves," *Pattern Recognit.*, vol. 40, no. 4, pp. 1282–1293, Apr. 2007.
- [62] L. Lam, S.-W. Lee, and C. Y. Suen, "Thinning methodologies—A comprehensive survey," *IEEE Trans. Pattern Anal. Mach. Intell.*, vol. 14, no. 9, pp. 869–885, Sep. 1992.
- [63] I. Demir, K. Koperski, and D. Lindenbaum, "DeepGlobe 2018: A challenge to parse the Earth through satellite images," in *Proc. Comput. Vis. Pattern Recognit.*, Jun. 2018, pp. 172–181.
- [64] J. R. Anderson, E. E. Hardy, J. T. Roach, and R. E. Witmer, "A land use and land cover classification system for use with remote sensor data," U.S. Geol. Surv., Reston, VA, USA, Tech. Rep. 964, 1976.
- [65] J. Fu *et al.*, "Dual attention network for scene segmentation," in *Proc. IEEE/CVF Conf. Comput. Vis. Pattern Recognit. (CVPR)*, Jun. 2019, pp. 3146–3154.
- [66] R. P K Poudel, S. Liwicki, and R. Cipolla, "Fast-SCNN: Fast semantic segmentation network," 2019, *arXiv:1902.04502*. [Online]. Available: <http://arxiv.org/abs/1902.04502>
- [67] H. Zhao, J. Shi, X. Qi, X. Wang, and J. Jia, "Pyramid scene parsing network," in *Proc. IEEE Conf. Comput. Vis. Pattern Recognit. (CVPR)*, Jul. 2017, pp. 2881–2890.
- [68] R. B. McMaster, "A statistical analysis of mathematical measures for linear simplification," *Amer. Cartographer*, vol. 13, no. 2, pp. 103–116, Jan. 1986.
- [69] Y. Liu, Z. Pei, Q. Wu, L. Guo, H. Zhao, and X. Chen, "Land use/land cover classification based on multi-resolution remote sensing data," in *Proc. Int. Conf. Comput. Comput. Technol. Agricult.* Berlin, Germany: Springer, 2011, pp. 340–350.



Yilang Shen was born in Xianning, Hubei, China, in 1991. He received the B.S. and Ph.D. degrees in geographical information systems from Wuhan University, Wuhan, China, in 2013 and 2019, respectively.

He is a Post-Doctoral Researcher at the School of Resource and Environmental Sciences, Wuhan University. His research interests include computer vision, map generalization, and change detection of spatial data.



Jingzhong Li was born in Macheng, Hubei, China, in 1983. He received the B.S., M.S., and Ph.D. degrees in geographic information systems from Wuhan University, Wuhan, China, in 2004, 2006, and 2009, respectively.

He is an Associate Professor at the School of Resource and Environmental Sciences, Wuhan University. His research interests include the multiscale representation of spatial data and geographic big data mining.



Rong Zhao was born in Wuwei, Gansu, China, in 1990. She received the B.S., M.S., and Ph.D. degrees in geographic information systems from Wuhan University, Wuhan, China, in 2014, 2016, and 2020, respectively.

She is a Research Assistant at the Chinese Academy of Surveying and Mapping, Beijing, China. Her research interests include the deep learning and pattern recognition.



Fengfeng Han was born in Datong, Shanxi, China, in 1988. She received the B.S. degree in geographic information systems from Shaanxi Normal University, Xi'an, China, in 2013, and the M.S. degree in geographic information systems from Wuhan University, Wuhan, China, in 2015.

She is an Engineer at Wuda Geo Information Technology Controls Ltd., Wuhan. Her research interests include the data analysis and social governance.